Circulation anomalies in boreal winter: Origin of variability and trends during the ERA-40 period

Diploma Thesis written by

Gereon Gollan
<ggollan@ifm-geomar.de>

IFM-Geomar Kiel

Kiel, December 13, 2011

Contents

Abstract

In this diploma thesis the interannual variability and trends of the winter mean tropospheric circulation in the northern hemisphere (NH) extratropics in winters from 1960/61 to 2001/02 are investigated. Output is analysed from a recent version of the atmospheric ECMWF model that has been used to perform various hindcast experiments, including experiments with selected regions of the atmosphere relaxed toward reanalysis data (ERA-40), i.e., the tropics and the stratosphere. The results are compared with the reanalysis data to examine the forecasting skill of the single experiments in the NH extratropics.

It is found that the stratosphere is influential on the interannual variability of the North Atlantic Oscillation (NAO) related part of the winter tropospheric circulation variability in the North Atlantic sector (NAS), but less important for other modes of variability in the NAS or over the North Pacific sector (NPS). The influence of the stratosphere on the NAO is thought to be caused by the downward propagation of circulation anomalies, for example, caused by sudden stratospheric warmings. Relaxing the tropical atmosphere is influential for the general circulation variability in the NAS, although the influence on the NAO is somewhat smaller than relaxing the global stratosphere. Both regions of the atmosphere therefore are important for a seasonal forecast in the NAS in winter. In the case of tropical relaxation, adding prescribed observed sea surface temperatures and sea ice (SSTSI) from reanalysis data improves the representation of the NAO in the model and is even more influential in reproducing the observed 42 year trend to a more positive NAO index. The stratosphere has a significant impact on the observed positive NAO trend only between 1964/65 and 1994/95, and in this period is comparable with the other forcings, the tropics and observed SSTSI. However, our model experiments are not able to account for more than 25% of the interannual variance of the NAO and not for more than 40% of the observed trend of the NAO in the ensemble means.

In the NPS the tropical atmosphere clearly has a strong impact on the interannual variability, and hence the seasonal predictability, which is measured here by means of the Pacific North America (PNA) pattern index. Single realisations of model experiments with tropical relaxation represent, on average, between 40% and 50% of the variance of the observed PNA pat-

tern. The ensemble mean with SSTSI from reanalysis data and no relaxation captures about 25% of the interannual variance of the observed PNA, but leads to a wrong trend in the PNA between 1960/61 and 2001/02 compared with the observations. The observed trend of the PNA is well captured in terms of the trend pattern if the tropics are relaxed to reanalysis data, except that the magnitude of the trend is reduced in the ensemble mean. It is remarkable that the observed PNA trend between 1960/61 and 2001/02 is also found to be within the range of trends of a control experiment, that sees the climatological mean cycles of SSTSI only. The strong impact of the tropical atmosphere on the extratropical atmosphere in the NPS is associated to the strong link between El Niño related variability in the tropical Pacific and the PNA that was confirmed by a number of previous studies.

Zusammenfassung

In dieser Diplomarbeit werden die zwischenjährliche Variabilität und Trends der mittleren Winterzirkulation in der Troposphäre der extratropischen Nordhemisphäre (NH) in Wintern von 1960/61 bis 2001/02 untersucht. Modellergebnisse von Hindcast Experimenten werden analysiert, die mit einer aktuelle Version des atmosphärischen ECMWF Modells durchgeführt wurden, unter anderem Relaxationsexperimente, in denen ausgesuchte Regionen der Atmosphäre, die Tropen und die Stratosphäre, an Reanalysedaten (ERA-40) angeglichen wurden. Die Ergebnisse werden dann mit Reanalysedaten verglichen, um die Vorhersagegüte der einzelnen Experimente in den Extratropen der NH zu bewerten.

Es wird herausgefunden, dass die Stratosphäre Einfluss auf die zwischenjährliche Variabilität der der Nord Atlantischen Oszillation (NAO) assoziierten Winterzirkulation im Nord Atlantischen Sektor (NAS) hat, jedoch weniger wichtig für andere Moden der Variabilität im NAS oder im Nord-Pazifischen Sektor (NPS) ist. Der Einfluss der Stratosphäre auf die NAO wird auf die Abwärtspropagation von Zirkulationsanomalien zurückgeführt, die zum Beispiel durch plötzliche Erwärmungen der Stratosphäre (SSW) verursacht werden. Die tropische Atmosphäre hat Einfluss auf die allgemeine Variabilität der Zirkulation im NAS, ist jedoch für die NAO Variabilität weniger wichtig als die Statosphäre. Beide Regionen der Atmosphäre sind daher im Winter wichtig für eine saisonale Vorhersage im NAS. Im Falle der tropischen Relaxation verbessert das Vorschreiben von Meeresoberflächentemperaturen und Meereisdaten (SSTSI) aus Reanalysedaten deutlich die Repräsentation der NAO im Modell und hat noch größeren Einfluss auf die Reproduktion des beobachteten 42-Jahres Trends zwischen 1960/61 und 2001/02 hin zu einem positiveren NAO Index. Die Stratosphäre hingegen hat nur zwischen 1964/65 und 1994/95 einen signifikanten Einfluss auf den positiven Trend der NAO, der dann mit dem Einfluss der anderen Forcings, den Tropen und SSTSI, vergleichbar ist. Unsere Modellexperimente können allerdings im Ensemblemittel nicht mehr als 25% der zwischenjährlichen Variabilität der NAO und nicht mehr als 40% des beobachteten Trends wiedergeben.

Im NPS hat die tropische Atmosphäre einen deutlichen und starken Einfluss auf die zwischenjährliche Variabilität, und damit die saisonale Vorher-

sagbarkeit, hier gemessen am Index des Pazifik-Nordamerika (PNA) Musters. Einzelne Modellläufe mit tropischer Relaxation geben im Durchschnitt zwischen 40% und 50% der Varianz des beobachteten PNA Musters wieder. Mit vorgeschriebenen SSTSI aus Reanalysedaten und ohne Relaxation gibt das Ensemblemittel 25% der zwischenjährlichen Varianz der beobachteten PNA wieder, liefert jedoch einen, verglichen mit den Beobachtungen, umgekehrten Trend zwischen 1960/61 und 2001/02. Der beobachtete PNA Trend hinsichtlich des Trendmusters wird mit tropischer Relaxation gut erfasst, nur die Amplitude des beobachteten Trends wird nicht erreicht. Es ist bemerkenswert, dass der beobachtete PNA Trend zwischen 1960/61 und 2001/02 auch innerhalb der Trends liegt, die von einem Kontrollexperiment erreicht werden, das nur mit mittleren klimatologischen SSTSI angetrieben wird. Der starke Einfluss der tropischen Atmosphäre auf die extratropische Atmosphäre im NPS wird mit der starken Verknüpfung von El Niño Variabilität im tropischen Pazifik und der PNA in Verbindung gebracht, die in vielen vorigen Studien bestätigt wurde.

Acronyms

AGCM	atmospheric general circulation model
AO	Arctic Oscillation
CLIM-NO	Climatological SST, no Relaxation
CLIM-STRAT	Climatological SST, Stratospheric Relaxation
CLIM-TROP10	Climatological SST, Tropical Relaxation, 10N-10S
CLIM-TROP20	Climatological SST, Tropical Relaxation, 20N-20S
COWL	"Cold Ocean Warm Land"
DJF	December, January, February
ECMWF	European Center for Medium-Range Weather Forecasts
ENSO	El Niño Southern Oscillation
EOF	Empirical Orthogonal Function
ERA	ECMWF Re-Analysis
GCM	general circulation model
GOGA	Global Ocean Global Atmosphere
NAM	Northern Annular Mode
NAO	North Atlantic Oscillation
NAS	North Atlantic Sector
NCAR	National Center for Atmospheric Research
NCEP	National Center for Environmental Prediction
NH	Northern Hemisphere
NOV	November persistence "experiment"
NPI	North Pacific Index
NPS	North Pacific Sector
OBS-NO	Observed SST, no Relaxation
OBS-TROP20	Observed SST, Tropical Relaxation, 20N-20S

PC	Principal Component
PDF	probability distribution function
PDO	Pacific Decadal Oscillation
PNA	Pacific North America
SAT	surface air temperature
SLP	sea level pressure
SST	sea surface temperature
SSTSI	sea surface temperature and sea ice
STD	standard deviation
SVD	Singular Value Decomposition
TOGA	Tropical Ocean Global Atmosphere
Z10	10 hPa geopotential
Z50	50 hPa geopotential
Z500	500 hPa geopotential

Chapter 1

Introduction and motivation

In meteorology, forecasting the weather to a maximum of accuracy is the main goal which everyone expects from a meteorologist. In the last years and with global warming being omnipresent in talks and media, climate's state has come into the awareness of society, too. For meteorologists and oceanographers understanding and forecasting global climate is of course one of the classic topics. Forecasting the state of the atmosphere and the ocean turns out to be very difficult, because the atmosphere is chaotic to a large extent. However, a lot of climate variability can be explained by large scale patterns, which may allow better predictability mostly due to the longer timescales of ocean dynamics. Some may also have a more or less oscillational character and so could give the possibility to make monthly to seasonal predictions. The El Niño Southern Oscillation (ENSO) phenomenon for example was found to have an oscillation character with a period of 2-7 years in the tropical Pacific, bringing either cold or warm surface water to the west coast of South America (Stoner et al., 2009).

Around the Pacific basin, ENSO can cause droughts or floods respectively and impact sea surface temperatures (SST) and mixed layer depths with influence on local fishery industries (Trenberth and Caron, 2000; Mantua et al., 1997). ENSO impacts atmospheric teleconnections patterns around the globe, for example the Pacific North America (PNA) pattern and perhaps also the North Atlantic Oscillation (NAO) both of which are extratropical atmospheric circulation patterns associated with fluctuations in the mid-latitude jet stream (Trenberth et al., 1998). Latif et al. (1994) note that at least the index of ENSO is predictable one year in advance.

Numerical models are the tool to make predictions for the future state of weather, ocean or climate on the one hand and on the other hand a possibility to make experiments to analyse impacts of forcings, to prove hypothesises of mechanisms. Extensive modeling studies confirmed the tropical influence in general, for example by prescribing tropical SSTs in an atmospheric general circulation model (AGCM), called Tropical Ocean Global Atmosphere

(TOGA) experiments. Trenberth et al. (1998) provide a comprehensive review of these studies. The response of the NAO to tropical SST remains questionable, although Greatbatch and Jung (2007) suggest a link between ENSO and the NAO at least for the period 1982-2001. It is important to note that both the NAO and the PNA showed distinct changes during the last decades, as the NAO showed a positive trend from the 1970s to the mid-1990's (Hurrell et al., 2004) and the PNA indicated a climate shift around 1977 to a deeper Aleutian low (Trenberth and Hurrell, 1994).

With improving observational data sets, longer observational time periods and sophisticated coupled general circulation models (GCMs), the interannual to interdecadal climate variability is thought to become better understood. The quality of global climate observations has strongly improved since the beginning of the satellite era. Besides that, the evolution of computer processors makes it possible to run a larger number of model runs which in turn become more complex and higher resolved.

Forcing the atmosphere can be done by "relaxing" atmospheric parameters like temperature and horizontal wind speeds to historically varying values from observations or reanalysis data in certain regions. This simulates a reduction of systematic errors in forecasts of climate models (Klinker, 1990). Jung et al. (2010) used this relaxation technique to examine the origins of the cold European winter 2005/2006.

In this thesis the relaxation approach is used to examine the origins of variability and trends in the extratropical circulation in boreal winters from 1960/61 to 2001/02, as explained in Chapter 2. The seasonal predictability is investigated by comparing the interannual variability of the model results with that of the observations from reanalysis data. The NAO index is studied as the indicator for the leading mode of variability in the North Atlantic sector and the PNA index is studied for the variability in the North Pacific sector. In the stratosphere, the Northern Annular Mode (NAM) index is analysed and the definitions of all indices are given in Sections 2.3 and 2.4. In Chapter 3 the methods for the analysis are explained and in Chapter 4 the results of the analysis are given, divided into the analysis of seasonal predictability in Section 4.1 and the analysis of climate trends during the ERA-40 period in Section 4.2. Conclusions and some discussion of the results are given in Chapter 5.

Chapter 2

Data and model

2.1 The ERA-40 reanalysis

Reanalysis datasets are a representation of collected data from station-based observations, ship data, ocean-buoys, radiosondes, aircraft and last but not least satellite data that have been assimilated into a dynamical model to create a physically consistent realisation available on all the standard atmospheric height levels. ERA-40 is provided by the European Center for Medium-Range Weather Forecasts (ECMWF) in Reading UK, and is an alternative to the popular US reanalysis data set provided by the National Center for Environmental Prediction (NCEP) and the National Center for Atmospheric Research (NCAR). For the ECMWF Re-analysis, ERA-40, the assimilation is done by combining observations from all sources with background information, while the background information is obtained by producing short-range forecasts of 6-h from the most recent previous analysis with an AGCM. The combination is done by minimizing the sum of error weighted measures of the deviations of the analysis from observed and background values. So the less observations available, the more the analysis data is dependent on the model physics . Sea surface temperature (SST) and sea ice data is taken from two main sources, the HADISST1 dataset until November 1981 and the NOAA/NCEP 2D-Var dataset until June 2001. After June 2001 data was taken from other NCEP products and interpolation was used to obtain daily values from each dataset (see Rayner (2001) for a discussion of the SST and sea ice fields used in ERA-40).

ERA-40 covers the period from September 1957 to August 2002 and is an approach to get the highest quality reanalysis possible after experience with former reanalysis data sets such as ERA-15 or NCEP/NCAR using a state of the art model to assimilate such data and to produce the background forecast.

The background forecast is produced by a model which was in use operationally from June 2001 to January 2002, but with a reduced resolution of

Table 2.1: *Some examples for spectral horizontal resolutions and their corresponding grid spacings. First column denotes the Spectral Triangular Truncation, second column the number of grid points in zonal direction n(lon) and number of grid points in meridional direction n(lat) of the corresponding regular Gaussian grid. Third column gives approximations of half of the smallest wavelength resolvable in km. Resolution of the model used to produce ERA-40 is T159 (bold).*

Truncation	n(lon) x n(lat)	grid resolution [km]
T63	190 x 95	211
T106	320 x 160	125
T159	**480 x 240**	**83**
T511	1534 x 767	26

T159 instead of the T511 used operationally. The spectral horizontal resolution of T159 is higher than in NCEP/NCAR (T62) and ERA-15 (T106) and corresponds to a grid resolution of 83km (see Table 2.1). It uses 60 levels in the vertical, whereas the resolution is higher in the planetary boundary layer and the stratosphere than in earlier models (see Figure 2.1), leading to a well-represented polar vortex in the stratosphere. The data assimilation was done with a 3D-Var system, which was introduced by the ECMWF in 1996, instead of the 4D-Var assimilation system which was operational when ERA-40 was produced. 6h assimilation periods were chosen to treat differences between analysis and observation time more consistently than with a 12h period. Uppala et al. (2005) provide more detailed information about the ERA-40 data set. Since its launch, the ERA-40 reanalysis dataset serves as a basis for model initialisations and as a global climate reference state in the period 1957 to 2002 (e.g. Stoner et al., 2009; Fueglistaler et al., 2009; Challinor et al., 2005).

In Figures 2.2 and 2.3 the winter climatologies for the winters 1961 to 2002 for the standard quantities sea level pressure (SLP), 500 hPa geopotential (Z500), 50 hPa geopotential (Z50) and 10 hPa geopotential (Z10) can be found taken from ERA-40. The most remarkable features in SLP are the Icelandic low in the North Atlantic, the Aleutian low in the North Pacific as well as the Siberian high extending over the Asian continent. At Z500 the shape of the climatology is more annular and shows the planetary Rossby waves of zonal wavenumber 3 in the jet stream. The average location and strength of the jet stream can be seen which is located where the contour lines have a large gradient; it is therefore stronger over the oceans and especially over the western boundary currents. In the stratosphere (Figure 2.3) the climatological mean patterns are even more annular and circumpolar, while their gradients are much larger than in Z500 which causes higher zonal wind speeds there.

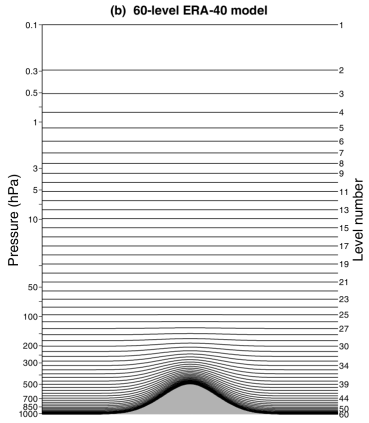

Figure 2.1: *Scheme of the 60 levels in the vertical used for the ERA-40 reanalysis at which the basic variables are represented. Nearly half of the levels of the model are located above the tropopause. From Uppala et al. (2005), Figure 4.*

In the following, anomalies of the observations are deviations from the corresponding climatology shown in these figures. Anomalies for the model runs are obtained by subtracting the model climatology calculated by averaging over all ensemble members and all years of the corresponding experiment. Those model climatologies are very similar to those of the observations and are therefore not shown. Nevertheless, this procedure ensures that the anomalies used do not reflect the different climates due to the model setup, but rather anomalous conditions corresponding to the individual winters.

2.2 The model

The goal of this study is to examine the predictive skill in the extratropics, if the forecast error is minimized in certain regions. Therefore the relaxation technique is used, which has proved to be a good tool to investigate the cause of circulation anomalies in previous studies. For example, Jung et al. (2011) found that the anomalously cold European winter 2009/2010 had its origin in the internal variability of the extratropical troposphere, whereas in winter 2005/2006, the tropics had a large impact on the anomalous circulation causing colder than normal conditions in Europe (Jung et al., 2010). Here, a similar analysis is done for the 42 winters from 1960/61 to 2001/02 to investigate the effect of a perfect forecast in different parts of the climate system for seasonal predictability, and also on climate trends in different regions.

An AGCM was used which was in use as the operational ECMWF model (cycle 36r1) from September 8th, 2009 to November 8th, 2010. The resolution was reduced to spectral truncation T159 (compared to the T1279

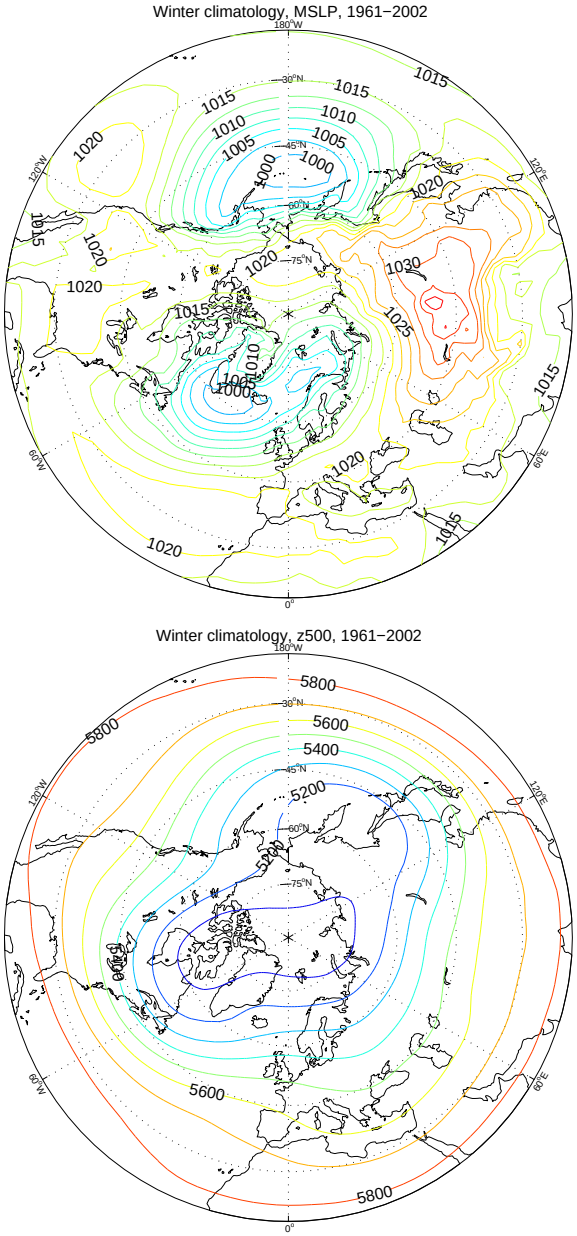

Figure 2.2: *ERA-40 Winter (DJF) mean SLP and* $500hPa$ *geopotential height 1961-2002. Contour interval is* $2.5hPa$ *for SLP and* $100m$ *for Z500 respectively.*

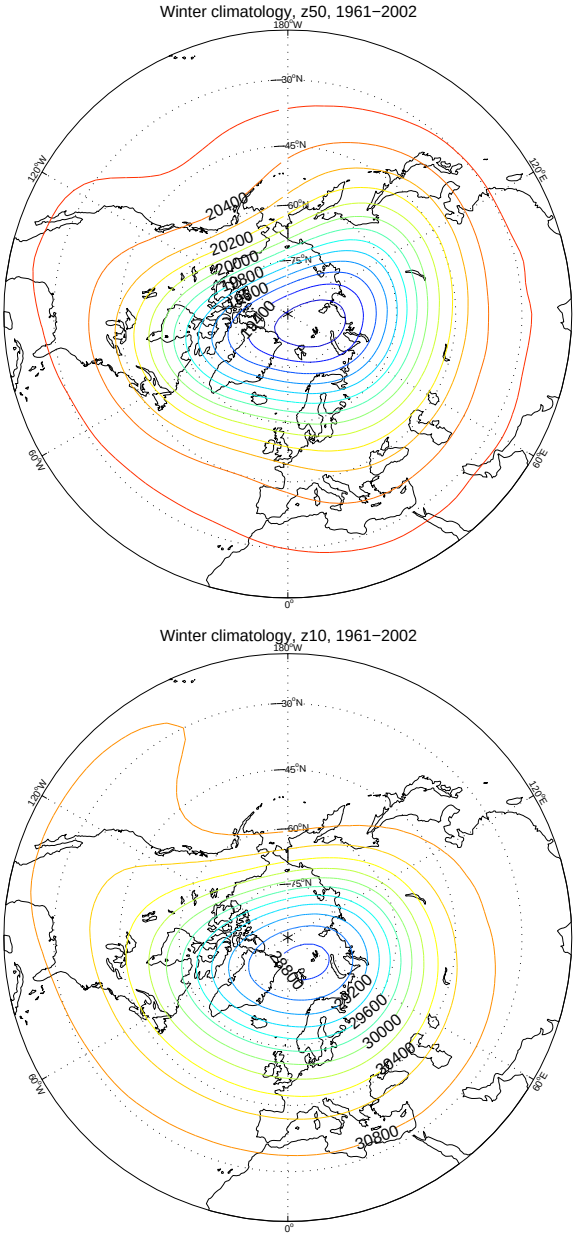

Figure 2.3: *ERA-40 Winter (DJF) mean* $50hPa$ *and* $10hPa$ *geopotential height 1961-2002. Contour interval is* $100m$ *for Z50 and* $200m$ *for Z10 respectively.*

used operationally) and 60 levels in the vertical reaching up to $0.1hPa$ (see Figure 2.1). For the analysis the data is truncated to T40, transformed to a Gaussian grid and then interpolated bilinearly to a regular 144×73 longitude-latitude grid with a resolution of $2.5° \times 2.5°$. In the relaxation experiments, an additional term was introduced to the model:

$$-\lambda(X - X_{ref}) \tag{2.1}$$

Here X represents the model state vector, X_{ref} the observed state of the atmosphere taken from ECMWF Re-Analysis (ERA)-40 to which the model is drawn and $\lambda = a\lambda_0$ specifies the relaxation coefficient. The ERA-40 reanalysis data thereby is available in the same horizontal and vertical resolutions in which our model was run so that no interpolation had to be applied at this stage. a specifies the region and vertical levels over which the relaxation is applied and $\lambda_0 = 0.1h^{-1}$ specifies the timescale of relaxation. In fact, the parameters relaxed are u, v, T and $\ln p_s$ (see following section for details).

For each experiment, an ensemble of 12 members is carried out separately for each winter. Averaging over the 12 ensemble members to produce the ensemble mean is done to eliminate the atmospheric noise. Initial conditions are taken from reanalysis data at the beginning of November for each year. The initial conditions of the ensemble members are consecutively picked with 6 hours lag from ERA-40 and the model is run from the beginning of November through February each year.

Unless stated otherwise, all the analysis is carried out on December, January, February (DJF) winter means so that, as an example, winter 1970 stands for the December 1969 to February 1970 mean. The boreal winter season was chosen because the northern hemisphere exhibits its greatest variability at this time of the year and also the NAO has most impact on European climate during winter.

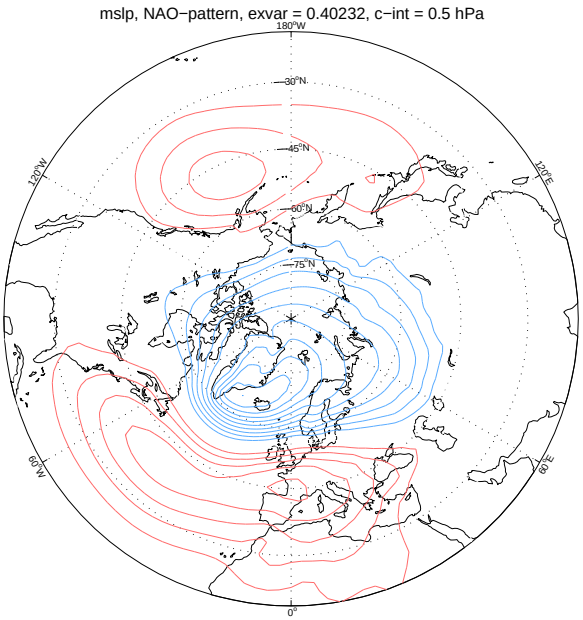

Figure 2.4: *An example for the internal variability of the model. The NAO pattern for CLIM-NO (climatological SST, no relaxation), obtained by regression of the modeled sea level pressure anomalies of all realisations of CLIM-NO to the model-NAO index (first PC) of an EOF-analysis (see Section 3.3) of SLP anomalies over the classic North Atlantic sector (*$20°N - 80°N$, $90°W - 40°E$, *defined by Hurrell (1995)). The variance explained by this pattern within the Atlantic sector is* 40.2%. *Contour interval is* 0.5 *hPa. Compare with Figure 2.7 which shows the NAO pattern obtained from reanalysis data.*

2.2.1 The different experiments

Climatological SST, no Relaxation (CLIM-NO):

As a reference model climate state, a set of integrations was computed with a climatological seasonal cycle of sea surface temperatures and sea ice (SSTSI) prescribed at the lower boundary. The climatology was obtained for the period 1979-2001 from ERA-40. Daily SSTSI fields were prescribed. Also insolation is in a climatological mean cycle in this experiment and in all other experiments described in the following. The members are independent from each other in this case since the runs only differ due to the initial conditions and therefore represent the internal variability of the model. These runs indicate the internal atmospheric variability as captured by the model, an example of which for the NAO is shown in Figure 2.4.

Observed SST, no Relaxation (OBS-NO):

Sea surface temperature and sea ice (SSTSI) impact the atmosphere mostly due to latent and sensible heat fluxes. A set of experiments forced with daily SSTSI taken from the ERA-40 reanalysis data set was produced

similar to the Global Ocean Global Atmosphere (GOGA) experiments described in Trenberth et al. (1998) with the difference that we simulate each winter separately while in GOGA continuous runs were performed over many years. The OBS-NO experiments assume a perfect forecast of SSTSI globally.

Climatological SST, Tropical Relaxation, 20N-20S (CLIM-TROP20):
Many studies found the tropical atmosphere to have an influence on the extratropics (see Chapter 1). Therefore a set of ensemble members is run, with the tropical atmosphere relaxed toward reanalysis data, including the tropical stratosphere, called CLIM-TROP20. This means that all model levels are relaxed within a belt from $20°N$ to $20°S$ at all longitudes. The relaxation coefficient λ_0 is $0.1h^{-1}$ which corresponds to a relaxation time scale of 10 hours. A hyperbolic transition is applied within a belt of 20° so that λ changes from zero at 30° to λ_0 at 10° N/S. Apart from the relaxation this experiment has the same setup as CLIM-NO. The same settings were used in Jung et al. (2010), where the authors tested the sensitivity of the results with respect to the value of λ_0 and the choice of the relaxation region. In the case of the 2005/2006 winter it was found that the results did not change substantially in the northern hemisphere with slightly different λ_0 and also slightly different relaxation boundaries.

Climatological SST, Tropical Relaxation, 10N-10S (CLIM-TROP10):
To test the robustness of the results regarding the choice of the relaxation region in this study, an additional experiment was executed for the tropical relaxation. So here the relaxation belt extends from $10°N$ to $10°S$ instead of $20°N$ to $20°S$ in CLIM-TROP20. Apart from that, the settings are the same in CLIM-TROP20 and CLIM-TROP10 and only four ensemble members were executed for CLIM-TROP10. However, the low number of members does not allow to completely average out the atmospheric noise by computing the ensemble mean.

Observed SST, Tropical Relaxation, 20N-20S (OBS-TROP20):
In this experiment SSTSI is taken from observations like in OBS-NO and the tropical atmosphere is relaxed toward reanalysis data from $20°N$ to $20°S$ like in CLIM-TROP20. A relaxation of the lowest layers of the tropical atmosphere wipes out the effect of tropical SST prescribed in CLIM-TROP20. This means that essentially, the extratropical SSTSI are "switched on" in OBS-TROP20 compared to CLIM-TROP20.

Climatological SST, Stratospheric Relaxation (CLIM-STRAT):
The stratosphere can impact the extratropical troposphere. This can happen due to changes in emitted or transmitted radiation due to changes in ozone and greenhouse gas concentrations on the one hand (see for example

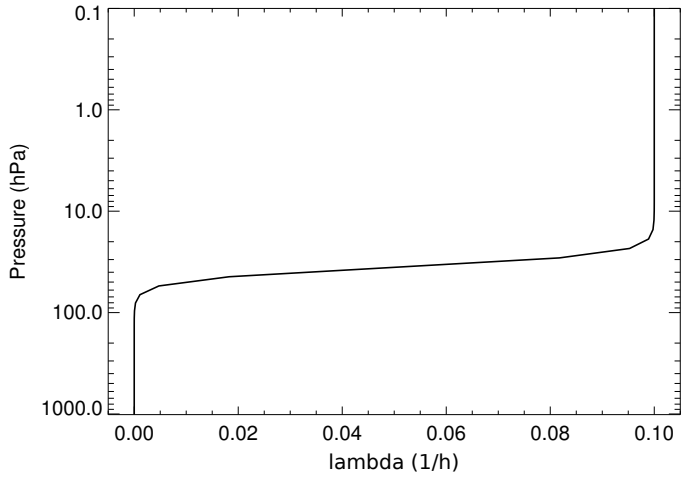

Figure 2.5: *Relaxation coefficient for the stratospheric relaxation in CLIM-STRAT. By courtesy of Prof. Thomas Jung.*

Thompson and Solomon (2002)). On the other hand, stratospheric circulation anomalies can propagate downward, leading to anomalous weather regimes in the troposphere (Baldwin and Dunkerton, 2001). To test the improvement of the forecast of extratropical circulation due to a perfect simulation of the stratosphere, an ensemble was run with the global stratosphere relaxed toward reanalysis data. The relaxation coefficient is smoothed over 13 height levels in the vertical using a hyperbolic tangent as transition in levels with the center of the transition located above the $100hPa$ level (see Figure 2.5). The values of λ at 500, 200, 50, and 20 hPa are given by $1.1 \times 10^{-7}\lambda_0$, $2.3 \times 10^{-6}\lambda_0$, $0.018\lambda_0$ and $0.5\lambda_0 hr^{-1}$, respectively. Surface pressure $\ln p_s$ is not relaxed in this case. Apart from the relaxation, this experiment has the same setup as CLIM-NO. For this experiment only the output for the tropospheric quantities SLP and Z500 are analysed as the stratospheric quantities Z50 and Z10 are effectively specified due to the relaxation.

November persistence "experiment" (NOV):

As another approach, the November anomaly fields taken from reanalysis data are used as a forecast of the following DJF assuming the anomalies persist unchanged. This "experiment" represents the most trivial method of seasonal forecasting, but can be used to examine how useful the other model experiments are.

A summary of the experiments can be found in table 2.2.

Table 2.2: *Short description of the experiments*

Abbreviation	model run	SST + sea ice	relaxation
CLIM-NO	✓	climatological	none
OBS-NO	✓	observed	none
CLIM-TROP20	✓	climatological	tropical, 20N-20S
CLIM-TROP10	✓	climatological	tropical, 10N-10S
OBS-TROP20	✓	observed	tropical, 20N-20S
CLIM-STRAT	✓	climatological	stratosphere
NOV	×	Nov anomaly persistence	

2.3 NAO and NAM - North Atlantic Oscillation and Northern Annular Mode

The NAO is the leading mode of variability in the North Atlantic Sector (NAS) and is therefore used in this thesis to investigate the variability in this sector (Greatbatch, 2000; Hurrell et al., 2003). It corresponds to fluctuations in the mid-latitude jet stream, the meridional displacement of storm tracks, the number of storms generated and the distribution of precipitation and temperature anomalies around the North Atlantic basin. The NAO pattern for SLP in boreal winter can be found in Figure 2.7. It represents the intensity of the typical Icelandic low and the Azores high pressure systems (at sea level), which are most pronounced in Boreal winter (DJF). Changes in the NAO can have a great impact on the densely populated areas of Western Europe, so that a lot of studies were done to investigate the variability of the NAO at all timescales (Hurrell, 1995; Semenov et al., 2008; Jung et al., 2011).

There are a lot of different ways to measure the state of the NAO. One of the oldest definitions is the normalised SLP difference between station measurements at or near the centers of action of the NAO, which are the Azores, Lisbon or Gibraltar for the center of high pressure and Iceland for center of the low pressure system, as defined by Hurrell (1995). This approach has the advantage of providing long time series, which can be derived back to the early 1820s due to long station records (Jones et al., 1997), but some features of the circulation pattern associated to the NAO do depend on the choice of the stations as there are several possibilities especially for the choice of the southern station. A more sophisticated measure of the NAO is the principal component of an Empirical Orthogonal Function (EOF)/Singular Value Decomposition (SVD) analysis of gridded SLP or Z500 anomaly data within the NAS, defined as the region bounded by $20°N - 80°N$, $90°W - 40°E$ (as defined by Hurrell, 1995). The large scale characteristics can then be found, for example the displacement of the centers of action over seasons and decades (Barnston and Livezey, 1987; Hurrell et al., 2003), but also

displacement between different NAO regimes (Peterson et al., 2003; Hilmer and Jung, 2000). The NAO can be defined by using geopotential heights of different pressure levels or by using sea level pressure fields.

In this thesis we will use geopotential heights of the $500hPa$ level and the region bounded by $30°N - 80°N$, $90°W - 40°E$ as the region to calculate the NAO. We change the southern boundary to 30^oN to avoid ambiguousness associated to the intersection of the analysis region and the region where relaxation was applied in the case of the tropical relaxation in CLIM-TROP20 and OBS-TROP20. The index corresponding to this definition (see Figure 2.6) is very strongly correlated to the standard NAO index

The NAM index expresses the extratropical variability throughout the whole northern hemisphere, so it has originally been defined as the principal component in SLP or geopotential height anomalies north of $20°N$ at all longitudes by Thompson and Wallace (1998). In the troposphere it is also referred to as the Arctic Oscillation (AO) index of which the corresponding pattern has separated centers of action of high pressure at mid latitudes and low pressure extending over the pole at high latitudes respectively. The NAM is more commonly used in the stratosphere, where the NAM index is a measure for the polar vortex and the patterns have a more annular shape. In the stratosphere, the annular mode is only present during winter, because during summer easterlies dominate in the NH extratropics due to the solar radiation which warms the polar stratosphere. For this thesis we define the NAM as the first PC north of 30^oN for the same reason as for the NAO (relaxation boundaries in the case of CLIM-TROP20 and OBS-TROP20) which is shown in Figure 2.6.

In Figure 2.6 some examples of different winter NAO and NAM indices are given, while in Figure 2.7 the regression pattern for the Principal Component (PC) - based NAO index in SLP (index (a) in Figure 2.6) and in Z500 (index (d)) can be found for the NAS north of 30^oN (see Chapter 3 for methods). On the one hand the robustness of the index in different methods, datasets and height levels can be seen as the indices all have a strong correlation. Only the NAM index for the stratosphere shows some independent variability in some years or periods, for example in the mid 1960s or the late 1990s, and is therefore less well correlated to the NAO index in SLP. On the other hand from the 1970s to the mid 1990s a trend to a more positive state can be seen, consistent with the findings by, e.g., Hurrell (1995); Thompson et al. (2000).

The NAO reveals a more or less white power spectrum. This does not exclude the possibility of having some decades with pronounced low frequency variability as noted by Wunsch (1999). For example we can find three consecutive low NAO winters during the late 1970s and five high NAO winters during the early 90s. These phases of "persistence" do not need to have any cause but can be produced by the chance of white noise.

In Figure 2.7 (top) the SLP NAO anomaly pattern shows the impact of a

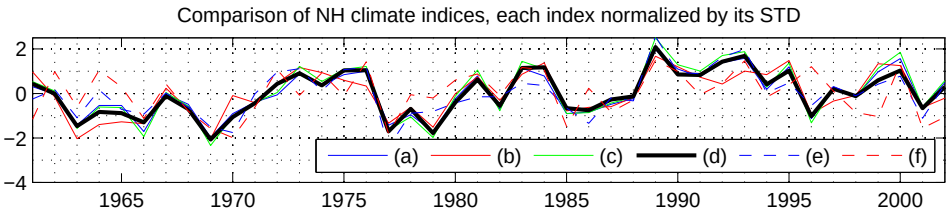

Figure 2.6: *NAO and NAM indices for the Northern Hemisphere (NH) calculated from ERA-40 reanalysis data except (c), which is Hurrell's index calculated from the NCEP/NCAR reanalysis dataset (downloaded from* `http://www.cgd.ucar.edu/cas/jhurrell/indices.data.html#naopcdjf`*).*
(a) NAO: first PC for SLP anomalies in Hurrell's sector: $20°N - 80°N$, $90°W - 40°E$;
(b) NAO: normalised SLP difference between the Azores $(37.5°N, 27.5°W)$ *and Iceland* $(65°N, 22.5°W)$;
(c) NAO: same as (a) but for NCEP/NCAR reanalysis data;
(d) NAO: first PC for 500hPa height anomalies in the NAS: $30°N - 80°N$, $90°W - 40°E$, *(used in this study);*
(e) NAM: as (d) but for the whole NH north of 30^oN;
(f) NAM: as (e), but for 50hPa height anomalies (lower stratosphere).

positive NAO index of +1 standard deviation, corresponding to index (a) in Figure 2.6. This index is the first PC of an EOF analysis of SLP data in the sector 20^oN - 80^oN and 90^oW - 40^oE. The negative anomaly corresponding to the Icelandic low has a minimum of $5hPa$ while the positive anomaly of the Azores high has a maximum of $4hPa$. In comparison with the Icelandic low and the Azores high in the SLP climatology in Figure 2.2 we can see that the centers of action of the NAO pattern are displaced northward. Additionally the negative anomaly corresponding to the Icelandic low extends more into the south in its eastern tail over the Eurasian continent. Due to geostrophy, the isobars can nearly be seen as the streamfunctions of the anomaly flow field, implying enhanced westerlies during high NAO phases in north-western Europe and western Russia. In Figure 2.7 (bottom) the regression pattern corresponding to index (d) (used in this study) for the $500hPa$ level is shown, obtained within the same sector as the SLP NAO pattern but with the southern boundary shifted from 20^oN to 30^oN. So, it can be seen that the patterns are very similar, only with the northern center of action shifted slightly westward at Z500 and extending further to the Pacific side of the pole than at mean sea level.

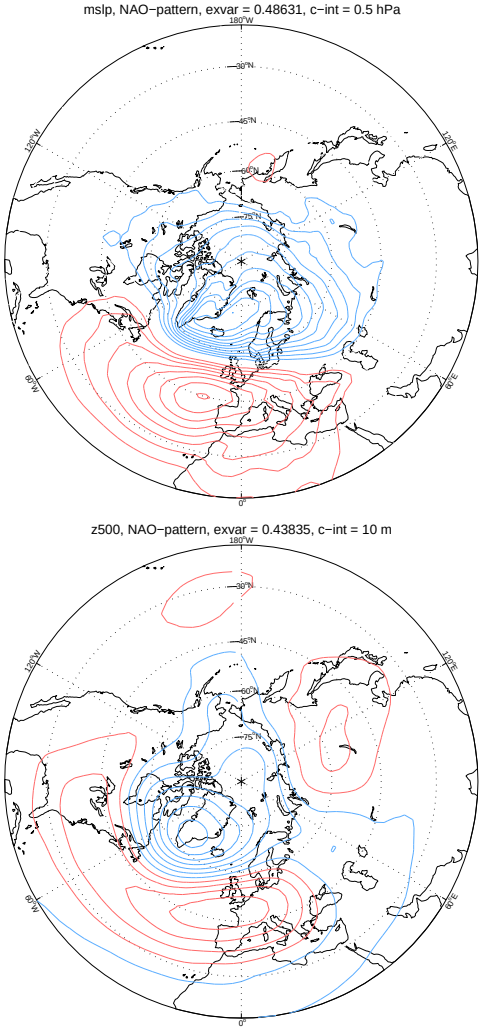

Figure 2.7: *NAO patterns for SLP (top) and Z500 (bottom). The pattern for SLP (Z500) is obtained by the regression of mean DJF SLP (Z500) anomalies from ERA-40 between 1960/61 and 2001/02 onto the observed NAO time series (a) shown in Fig. 2.6 (index (d) for Z500). The variance explained by this pattern within the Atlantic sector in winter is* 48.6% *(*43.8%*). Note that the patterns are similar, although referring to different heights and are based on different sectors for the calculation (*20^oN - 80^oN *for SLP and* 30^oN - 80^oN *for Z500,* 90^oW - 40^oE *for both heights). Contour interval is* 0.5 *hPa* (10m).

2.4 PNA - Pacific North America pattern

The PNA index is the counterpart of the NAO in the extratropical Pacific and basically measures the strength of the Aleutian low. It is the mode of variability in the North Pacific which corresponds to the distribution of SLP, surface air temperature (SAT) and precipitation anomalies around the North Pacific basin as well as to SST and sea ice (SSTSI) anomalies and mixed layer depths in the North Pacific. It is closely connected to other North Pacific indices, such as the North Pacific Index (NPI) or the Pacific Decadal Oscillation (PDO) (SST index), c.f. Mantua et al. (1997). As an indicator of interannual variability in the troposphere with focus on the North Pacific, we choose the PNA index here to examine the skill of the relaxation experiments in this sector.

The PNA index was originally defined as a four point index of 500hPa height anomalies, including the Aleutian low and the corresponding ridge over Canada (see Wallace and Gutzler (1981)). The PNA index has been revised to several versions, such as a weighted area mean of SLP over the North Pacific sector ($160°E - 140°W$ and $30°N - 65°N$, NPS, suggested by Trenberth and Hurrell (1994)). This index is used in this study and also the minus of the weighted area mean of $500hPa$ height anomalies over the same sector.

In modelling studies and also in observations it was found that the Aleutian low is deeper (positive PNA index) during a warm ENSO event (Trenberth and Caron, 2000; Alexander et al., 2002). This is caused by the excitation of Rossby waves due to anomalies in equatorial convection which transport momentum to the mid-latitudes, enhancing westerlies in the latitude band $20° - 40°$ in both the North and South Pacific. These extratropical atmospheric anomalies can in turn influence surface heat fluxes and therefore SSTs in the North Pacific. The remote connection between tropical SSTs and extratropical SSTs has been called an "atmospheric bridge" (Alexander et al., 2002).

It was found that North Pacific climate underwent a shift around the late 1970s towards a deeper Aleutian low and therefore a higher PNA index. This caused for example lower surface temperatures (and SSTs) in the central North Pacific, higher temperatures in the Alaskan region resulting in warmer SSTs and diminishing Salmon stocks thereafter (Trenberth and Hurrell, 1994; Mantua et al., 1997). A number of remote teleconnections associated to the Pacific such as the connection between ENSO and European winter climate show a regime shift from the period before the late 1970s and afterwards (Greatbatch et al., 2004).

In Figure 2.8 five different Pacific indices can be found. Indices (a), (b),(c) and (d) indicate North Pacific atmospheric variability, derived from ERA-40 reanalysis data and show high correlation between different methods

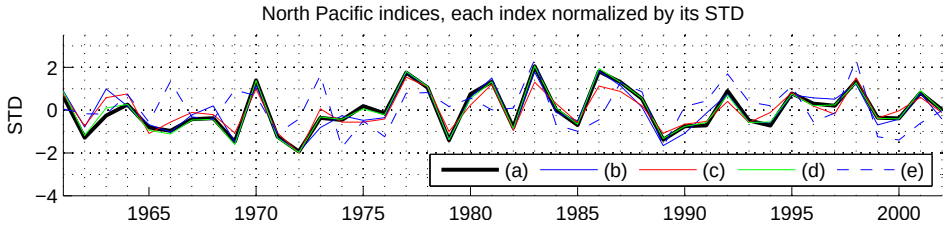

Figure 2.8: *Normalised North Pacific climate indices, all from ERA-40:*
(a) negative of PNA index, the weighted area mean of 500hPa anomalies over the North Pacific sector: $30°N - 65°N$, $160°E - 140°W$ *defined by Trenberth and Hurrell (1994);*
(b) negative of NPI index which is the weighted area mean of SLP anomalies over the same sector as for (a);
(c) PNA 4-point index defined by Wallace and Gutzler (1981) as: $PNA = \frac{1}{4}[z^*(20°N, 160°W) - z^*(45°N, 165°W) + z^*(55°N, 115°W) - z^*(30°N, 85°W)]$ *with* z^* *being the 500hPa height anomalies normalised by their standard deviation;*
(d) first PC of an EOF analysis of 500hPa anomalies over the same sector as for (a);
(e) Niño 3.4 SST index, data from NCAR (original time series (1871-2007): `http://www.cgd.ucar.edu/cas/catalog/climind/TNI_N34/index.html#Sec5`*) and normalised by its standard deviation for winters from 1961-2002.*

and heights in the troposphere. Index (e) is the El Niño 3.4 index suggested by Trenberth (1997), which is defined as the 5-month running means of SST averaged over the area ($120°W - 170°W, 5°S - 5°N$) and calculated from NCEP/NCAR SST data (data from `http://www.cgd.ucar.edu/cas/catalog/climind/TNI_N34/index.html#Sec5`). It is interesting to see that the correlation between the Niño 3.4 and the PNA index is low in the first half of the entire period (i.e., 0.26) and high in the second half (0.60). The change in correlation is probably connected to the climate shift in the late 1970s changing the impact of tropical SSTs on the extratropical atmospheric circulation in the Pacific sector. This shift can also be seen in Figure 2.8. Before 1977, only two winters of a positive PNAm index were found, whereas in the following twelve years nine winters of a positive and only three of a negative PNA index were found, the positive PNA winters being much more pronounced thereby. After 1988 the PNA went to a more balanced phase with only two winters which exceeded one standard deviation in the PNA index.

In Figure 2.9 the regression pattern of index (a) can be found, showing the positive phase, corresponding to +1 standard deviation, of the PNA pattern in $500hPa$ with the trough over the North Pacific associated to the Aleutian low and a ridge over Canada.

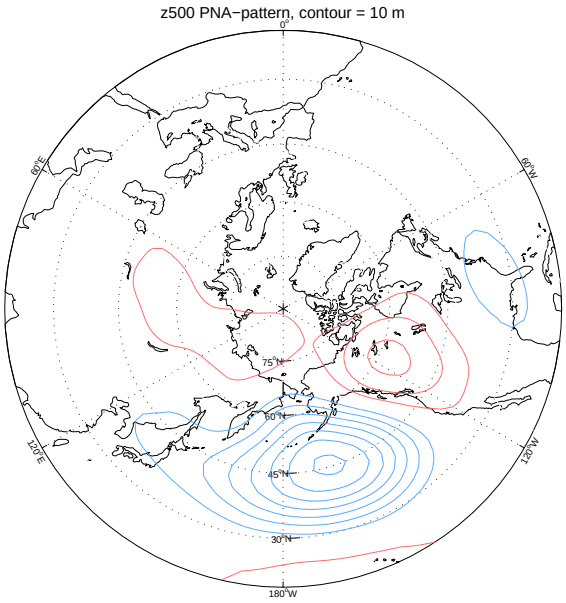

Figure 2.9: *PNA pattern obtained by regression of observed (ERA-40, 1960/61 to 2001/02) DJF 500hPa height anomalies onto the observed PNA time series (a) shown in Fig. 2.8. The variance explained by this pattern within the North Pacific sector in winter is* 53.5%. *Contour interval is* $10m$.

Chapter 3

Methods

3.1 Linear regression and correlation

If x and y are continuous random variables of length T, the evolution of y can be estimated in a linear-least-square sense if x is assumed to be known with precision:

$$\hat{y} = a_0 + a_1 \cdot x + \varepsilon \tag{3.1}$$

with some uncertainty, expressed by the error ε. Then the linear regression coefficient a_1 which estimates the dependence of y on the regressor x is

$$a_1 = \frac{\overline{x'y'}}{\overline{x'^2}} \ , \tag{3.2}$$

where $x' = x - \overline{x}$ are anomalies deviating from the arithmetic mean $\overline{x}$. Here and in the following all notations defined for x are also valid for y. The covariance of x and y is defined by:

$$Cov_{xy} = \overline{x'y'} = \frac{1}{T-1} \sum_{t=1}^{T} x'y' \tag{3.3}$$

Another measure of the relationship between x and y is the correlation ρ_{xy}, which assumes uncertainties for both variables:

$$\rho_{xy} = \frac{\overline{x'y'}}{\sigma_x \sigma_y} \ , -1 \leq \rho \leq 1 \tag{3.4}$$

where σ_x is the standard deviation (STD) of x, the square-root of the variance of x, $Var(x)$:

$$\sigma_x = \sqrt{Var(x)} = \sqrt{\frac{1}{T-1} \sum_{t=1}^{T} (x')^2} \tag{3.5}$$

ρ_{xy}^2 is the fraction of explained variance of y explained by x in a linear least-square sense and vice-versa.

3.2 Weighting and projection

When working with geographical maps on a sphere, one often has to consider the latitudinal dependence of the size of the grid boxes. Otherwise in projections or covariances, the gridboxes near to the poles are given too much weight as the number of gridboxes increases towards the poles on many types of grids. The results of any analysis should be independent of the choice of the grid type. For a regular longitude-latitude grid, weighting is done by multiplying the value at each grid point with the cosine of its corresponding latitude θ. To explain the method in matrix notations, an area-weighting matrix can be defined as a diagonal matrix with the same size as the covariance matrix of the data. In the case of a data set X stored on a regular longitude-latitude grid with m longitudes and n latitudes from T observational time steps

$$X \, \epsilon \, \mathbb{R}^{m \times n \times T} \ .$$

There are $S = m \cdot n$ grid points so that the spatial dimensions of X can be merged to one dimension:

$$X \, \epsilon \, \mathbb{R}^{S \times T}$$

Then the weighting matrix is (see Baldwin et al. (2009))

$$W \, \epsilon \, \mathbb{R}^{S \times S}, \ W_{ij} = cos(\theta)\delta_{ij} \tag{3.6}$$

with the Kronecker delta defined as

$$\begin{aligned} i = j &\Rightarrow \delta_{ij} = 1 \\ i \neq j &\Rightarrow \delta_{ij} = 0 \ . \end{aligned}$$

This is in fact the weighting matrix we will use throughout the present study. For example before computing the variance of X the data has to be multiplied with the square-roots of $cos(\theta)$, expressed here as the weighting matrix $W^{1/2}$:

$$X_w = W^{1/2} \cdot X \tag{3.7}$$

$$var(X) = \frac{1}{T-1} \left(X'_w \cdot X_w^{'\,t} \right) \tag{3.8}$$

X^t denotes the transpose matrix of a matrix X. If $\overline{X}$ is the time average of X, $X' = X - \overline{X}$ is the anomaly field.

Projections examine the linear dependence of one vector or field on another one. If X and Y are fields of the same length S, this is done by calculating the scalar product of the weighted fields:

$$\langle X_w \mid Y_w \rangle = \sum_{i=1}^{S} X_{w,i} Y_{w,i} \quad \epsilon \, \mathbb{R} \tag{3.9}$$

With other grid types, such as Gaussian grids, the weighting matrix W contains values other than $cos(\theta)$ and its elements can be taken from reference tables.

3.3 Empirical orthogonal functions (EOF)

The EOF analysis is a method to decompose any data set into linearly independent modes. In climate dynamics EOFs can be used to derive theories for mechanisms or to extract reoccuring and therefore possibly predictable phenomena. Other applications also make use of the EOFs, e.g., the jpg format for images uses a limited number of EOF modes of an image to present the image using a smaller data set. A detailed description of the EOF problem and derivation of the connections explained below can be found in von Storch and Zwiers (2001).

Let D be a climate data set with m longitudes, n latitudes and T observations.

$$D \, \epsilon \, \mathbb{R}^{m \times n \times T}.$$

The EOFs are based on the covariance matrix of the field, so the spatial dimensions have to be merged to obtain a two dimensional matrix for D:

$$D \, \epsilon \, \mathbb{R}^{S \times T}$$

with $S = m \cdot n$. Additionally, as explained in Section 3.2, the field has to be weighted with $W^{1/2}$ when considering variances and the temporal mean has to be removed so that the elements of the covariance matrix of D are

$$cov(D)_{ij} = \frac{1}{T-1} \sum_{t=1}^{T} D'_{it,w} D'_{jt,w}. \tag{3.10}$$

$cov(D)$ is symmetric and has the dimensions $cov(D) \, \epsilon \, \mathbb{R}^{S \times S}$. The EOFs are then the eigenvectors $\vec{e_i}$ of the covariance matrix of D which have unit length (Euclidean norm) and together with the eigenvalues λ_i solve the eigenvalue problem

$$(cov(D) - \lambda_i I_S) \, \vec{e_i} = 0 \tag{3.11}$$

where I_S is the identity matrix with the size of $cov(D)$. There are S eigenvectors which can be written as the rows of a matrix E and the corresponding eigenvalues can be written as one vector $\vec{\lambda}$:

$$E \, \epsilon \, \mathbb{R}^{S \times S} \tag{3.12}$$

$$\vec{\lambda} \, \epsilon \, \mathbb{R}^{S} \, . \tag{3.13}$$

There are S eigenvalues of which r are non-zero and it can be shown that

$$r = rank(cov(D)) = \frac{S \cdot T}{S + T} \tag{3.14}$$

which means that if one of S or T is much larger than the other, r will converge towards the smaller one. In our case 42 winter means define the time dimension and a much larger amount of grid points ($O(10000)$) is given, it follows from (3.14) that $r \approx T = 42$. The corresponding principle component (PC) time series can be obtained by projecting (see Section 3.2) the weighted anomaly fields D_w onto the EOF patterns (which are already weighted) for every timestep which can be expressed by the matrix multiplication:

$$PC = E \cdot D_w \ . \tag{3.15}$$

The PC time series are then given as a matrix which has S rows and T columns:

$$PC \ \epsilon \ \mathbb{R}^{S \times T}$$

The dataset D at any timestep t can then be reconstructed by the linear combination of the EOF modes:

$$D_t = \sum_{i=1}^{S} PC_{it} \ \vec{e_i} \tag{3.16}$$

From the definition it follows that the modes are characterised by the orthogonality of the spatial patterns, i.e.

$$\langle \vec{e_i} | \vec{e_j} \rangle = 0 \qquad \forall \ i \neq j \tag{3.17}$$

and that their time series are uncorrelated, i.e.

$$\rho_{PC_i PC_j} = 0 \qquad \forall \ i \neq j \tag{3.18}$$

The variance of D is the sum of the eigenvalues of the covariance matrix, while each eigenvalue λ_i is the variance explained by the corresponding eigenmode:

$$var(D) = \sum_{i=1}^{S} \lambda_i \Rightarrow explained \ variance[\%] = \frac{\lambda_i}{Var(D)} \tag{3.19}$$

For the presentation of the EOFs the spatial patterns $\vec{e_i}$, which have unit length, are multiplied by the standard deviation of each mode $\sigma_i = \sqrt{\lambda_i}$ to obtain the patterns in the same dimensions as the data itself, whereas the time series are normalised by their standard deviation:

$$\vec{e_i}^* = \sqrt{\lambda_i} \vec{e_i} \tag{3.20}$$

$$PC_i^* = \frac{1}{\sqrt{\lambda_i}} PC_i \tag{3.21}$$

The sign of an EOF pattern is thereby arbitrary and can be changed simultaneously with that of its PC time series to consider its climatological

relevance. It is important to note that the results of an EOF analysis have to be interpreted with caution since the constraint of orthogonality in space can lead to spurious results especially in the higher order EOFs. These do not have to be consistent with the natural modes of variability (Dommenget and Latif, 2002). However, the EOF modes presented in this study and used for the analysis have a maximum order of two and have been proved to agree with the results from different methods as described in Sections 2.3 and 2.4. They can therefore be interpreted as "real" physical modes.

3.4 Pattern correlation

To compare the spatial structure of two patterns regarding their linear dependence without considering the amplitude, one can calculate the pattern correlation. The weighted area mean of each of the patterns $X, Y \epsilon \mathbb{R}^S$ has to be subtracted:

$$\hat{X} = X - \left(\frac{\sum_{i=1}^{S} \cos(\theta_i) X_i}{\sum_{i=1}^{S} \cos(\theta_i)} \right) \tag{3.22}$$

It is important again that the patterns are weighted before computing the correlation (see Section 3.2). In this case the weighting is done with $W^{1/2}$:

$$\hat{X_w} = W^{1/2} \hat{X} \tag{3.23}$$

The correlation is then calculated as defined in Section 3.1:

$$\rho_{patt}(X, Y) = \frac{\sum_{i=1}^{S} \hat{X_{w,i}} \hat{Y_{w,i}}}{\sigma_{\hat{X_w}} \sigma_{\hat{Y_w}}}; \tag{3.24}$$

An illustration of pattern correlation can be found in Figure 3.1.

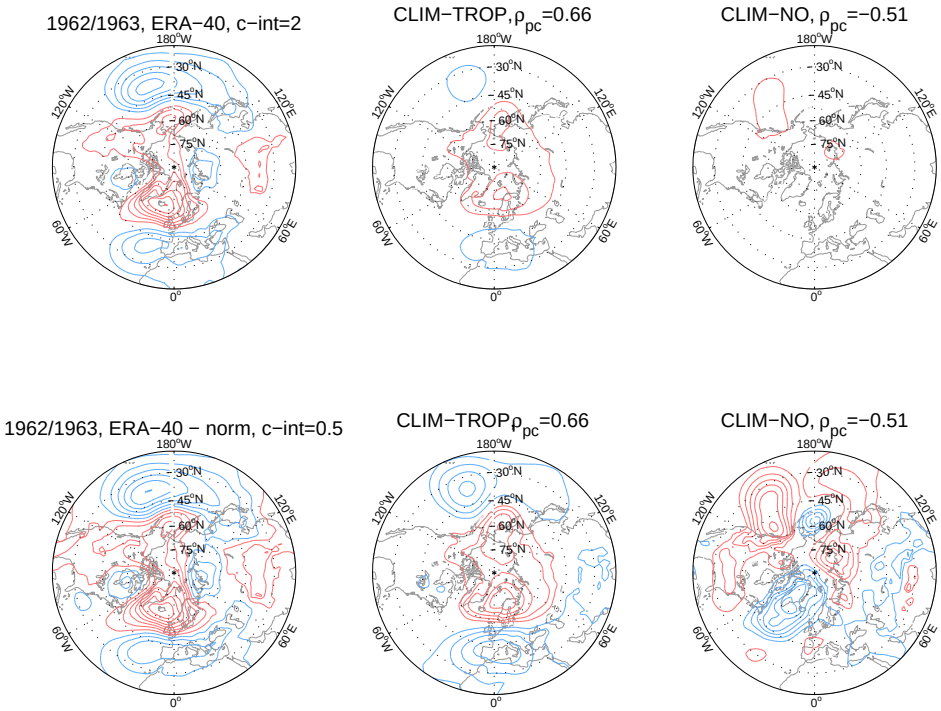

Figure 3.1: *SLP anomalies in the NH for winter 1962/1963, first row showing the observed anomalies and ensemble means (CLIM-TROP20 and CLIM-NO) and second row showing the anomalies for which the area mean of each pattern has been subtracted as described in Section 3.4, equation (3.22). Furthermore, each pattern is normalized by its weighted standard deviation to show only those features of the pattern which are relevant for ρ_{patt}. ρ_{patt} between the ensemble mean and reanalysis data is given in the figure. Contour interval in the first row is $2hPa$ and 0.5 in the second row.*

3.5 Monte Carlo methods

To test the significance of statistical parameters like trends and correlations of continuous random variables, Monte Carlo methods are applied. This method can be used as an alternative to the Student's t-test and is called "Monte Carlo", referring to the games of chance commonly played in Monte Carlo, Monaco, and was first described by Metropolis and Ulam (1949). The Monte Carlo method is based on the assumption that the average of the results comes closer to the theoretically expected value the larger the number of trials that are used (the law of large numbers; Hsu and Robbins (1947)). In the following we use the NAO index as an example. This method involves generating time series of the NAO index from the model results with which to compare the observed time series. The Monte Carlo method is best illustrated by examples.

Case 1: Is the correlation between the ensemble mean NAO index from a particular model experiment and the observed NAO index significantly different from zero?

- 12 artificial time series of the NAO index are produced by randomly selecting (without replacement) 42 values 12 times from the original $12 \times 42 = 504$ values available from the model results. The ensemble mean NAO index is then calculated from the selected values for each year and the correlation between the times series of this ensemble mean index and the observed NAO is computed. The process is then repeated a large (typically 10,000) number of times and a histogram of the ensemble mean values is computed to produce the probability distribution function (PDF) of the correlation values. All histograms have 50 bins and are normalized to have an integral of 1.
- The resulting PDF is centered around zero and significance levels can be derived by calculating the correlation ranges corresponding to percentiles, e.g., the 5% or 95% percentiles. The significance of the correlation between the actual ensemble mean NAO index from the model experiment and the observed index can then be assessed by noting into which percentile it falls.
- The results agree with Student's t-test if 42 degrees of freedom are assumed. Serial correlation (memory from one winter to the next) would reduce the number of degrees of freedom and increase the threshold correlations for significance. Although not thought to be a serious problem for the NAO and the PNA, this possibility should be kept in mind when interpreting the results.

Case 2: How unusual is the observed NAO trend in the context of an particular model experiment?

- A large number (e.g., 10000) of time series of the NAO index are produced by picking one value for the NAO index from the 12 original members for each year, keeping the order of the years as in the original experiment. Noting that the real world corresponds to a single realization, it is clear that any of the selected realisations could correspond to the observed NAO time series within the context of the particular model experiment. The trend is then computed for each realization and a PDF of trends is produced as described above for the correlation values.
- The PDFs of all cases will, to a good approximation, be centered around the trend of the original ensemble mean NAO index from

the experiment and it can then be seen into which percentile of the PDF the observed trend falls.

Case 3: Which correlations between the time series of the NAO index of single realisations and the observed NAO index are possible? How strong is the added forcing in each experiment?

- Possible realisations are produced as for the trends above and the correlation between the NAO index of the new realisations and the observed NAO index is calculated to produce a PDF of these correlations.
- The resulting PDF is centered around a correlation value which is lower than the correlation of the ensemble mean NAO index with the observed one (see Bretherton and Battisti (2000)).
- Depending on how much the resulting PDF is shifted away from zero one can conclude how strong the added forcing is. Likewise, these PDFs give an indication of how realistic the model simulations are compared to the observations. The more the PDF is shifted towards positive correlations, the more realistic the corresponding model setup represents the variability of the real world in our period.

In all cases, the shuffling is carried out by randomly selecting numbers from a uniform distribution of integers between 1 and 12 or 1 and 42 respectively.

Chapter 4

Results

The results of our model experiments will be presented by means of comparison with the reanalysis data set ERA-40 (hereafter referred to as the observations). There are separate sections for the analysis of interannual variability as a measure of the seasonal forecasting skill of the different experiments (Section 4.1), and the investigation of trends during winters from 1961 to 2002 (Section 4.2). First of all it is useful to say that our model (an AGCM, see Section 2.2) reveals similar modes of variability compared to the observations if, for example, an EOF analysis is carried out as for the observations. See Figures 2.4 and 2.7 for comparison of the NAO patterns obtained from the "control" experiment CLIM-NO and the observations. The model therefore represents well the internal variability of the real atmosphere and it is consistent to produce NAO/PNA indices for the experiments by projecting the model anomaly fields onto the spatial patterns which result from the analysis of the observational data (see Chapters 2 and 3 for details).

As a measure of the model's skill to produce a seasonal forecast, pattern correlations between fields from observations and ensemble member fields are used in Section 4.1. The correlations between the observed NAO (PNA) index and the model NAO (PNA) indices are discussed in Sections 4.1.1 and 4.1.2. The correlation measure does not consider the variance of each time series, but it is a measure of the tendency of both indices to vary coherently and of the constancy of the ratio of their magnitudes. The correlation over the whole period is a measure of the capability of the model to forecast the winter mean value of the given index. In Figure 4.1 a schematic summary of the results of the correlation analysis corresponding to ensemble means can be found for the $500hPa$ geopotential heights.

In Section 4.2 trends are investigated in terms of their patterns and also their amplitude. Figure 4.2 gives a summary of the results of the trend analysis in terms of the amplitude of the NAO and PNA trend which is represented by the different experiments.

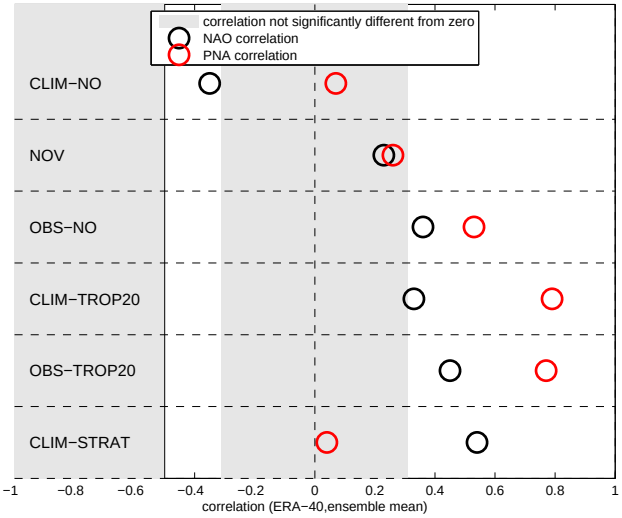

Figure 4.1: *Schematic summary of the correlations between the observed NAO/PNA index and the NAO/PNA index of the ensemble means at 500hPa. NAO index (black circles) and PNA index (red circles). A description of the experiments can be found in Section 2.2.1. Correlations lower than 0.31 are not significantly different from zero, as they lie within the 95% confidence interval according the results of the Monte Carlo simulations explained in Section 3.5. In Sections 4.1.1 and 4.1.2 it is found that the significance levels do not differ substantially between the experiments and for either the NAO or PNA index.*

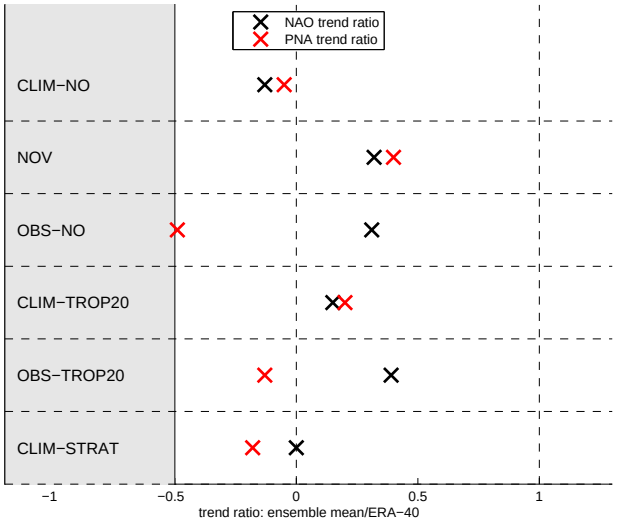

Figure 4.2: *Schematic summary of the analysis of the trends of the NAO and PNA indices at 500hPa. NAO index (black crosses) and PNA index (red crosses). The ratio of each ensemble mean trend with the observed trend is shown, so the closer the ratio is to 1, the better the representation of the trend in the corresponding experiment. A description of the experiments can be found in Section 2.2.1 and especially Table 2.2.*

4.1 Seasonal forecasting

In Figures 4.3 and 4.4 the pattern correlations ρ_{pc} of Z500 anomalies of ensemble members with the observed anomalies from the corresponding years are summarised as histograms. The histograms of all 42 winters and all 12 ensemble members are shown to examine which spatial correlations occur most frequently for the selected experiments and the sectors of interest. However, for the persistence "experiment" NOV only 42 values are available. The pattern correlation shows the skill of the model to forecast the mean winter circulation and shows which forcing has the largest effect. The average of the pattern correlations at $500hPa$ for all years for all ensemble members for the NH ($\geq 30^o$N), the NAS ($30°N - 80°N$, $90°W - 40°E$) and the North Pacific Sector (NPS) ($30°N - 65°N$, $160°E - 140°W$) are shown in Table 4.1. In Table 4.2 the fraction, i.e., the probability of positive pattern correlations for the whole set of realisations of each experiment is noted.

In the Northern Hemisphere (NH), the values for CLIM-NO and NOV resemble a normal Gaussian distribution with mean zero (Fig. 4.3, Table 4.1) The results are very similar in the NAS and the NPS (only shown in the tables). The fraction of positive ρ_{pc} is around 50% for the ensemble members of both experiments, which indicates that there is no forecast skill using these methods.

For the experiments with tropical relaxation, the ensemble members generally yield higher pattern correlations compared to the other cases and the highest values occur with tropical relaxation in OBS-TROP20 in all sectors, especially in the NPS where the spatial correlation is $\overline{\rho_{pc}} = 0.45$ in the average. However, it is noticeable that for CLIM-TROP20, where SSTs are in a climatological cycle, the pattern correlations of the single realisations are of a similar magnitude as those of OBS-TROP20 ($\overline{\rho_{pc}} = 0.40$ in the average in the NPS) and it can be concluded that the origin of the high correlation is located in the tropics rather than in the prescribed extratropical SST and sea ice (SSTSI). For the tropical relaxation experiments, $80 - 90\%$ of the realisations yield positive pattern correlations if the NH and the NPS are considered. In the NAS only $60 - 70\%$ of ρ_{pc} are positive, indicating that the tropical forcing is still not enough to represent the variability, but nevertheless has a clear impact compared to CLIM-NO and NOV.

In Figures 4.3 and 4.4 the results for CLIM-STRAT realisations are also shown. Stratospheric relaxation has little influence in the NPS as the pattern correlations are nearly equally distributed with some kurtosis so that large positive and negative ρ_{pc} are likely, suggesting a bimodal response to the stratosphere . For the NH and NAS, CLIM-STRAT slightly shifts the correlations to positive values and with a normal-like distribution (see Figure 4.4 and Table 4.1). Slightly more than 50% of ρ_{pc} are positive (Table 4.2). In the NAS both CLIM-TROP20 and CLIM-STRAT have their mean shifted to positive values while CLIM-TROP20 is in the average higher ($\overline{\rho_{pc}} = 0.15$)

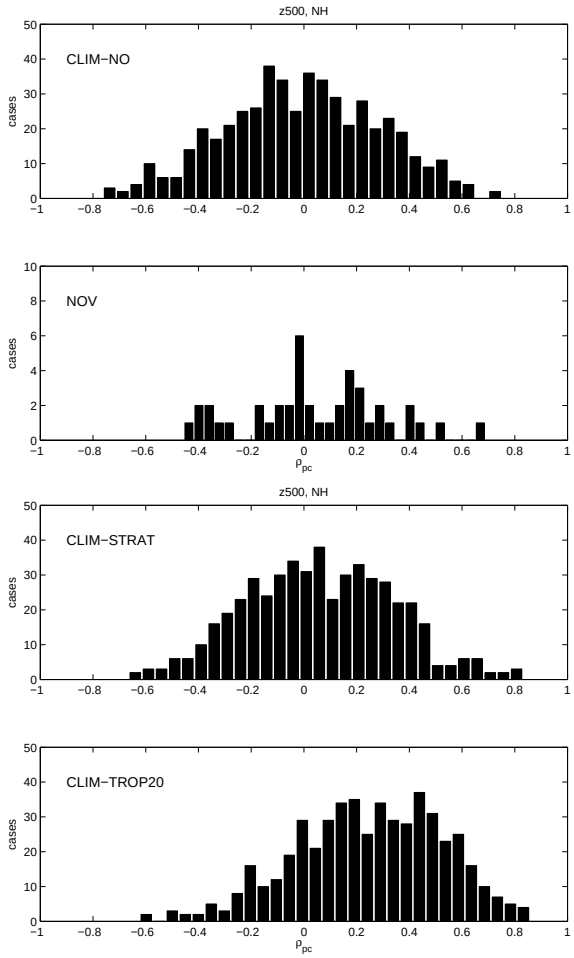

Figure 4.3: *The histograms of pattern correlations between observations and November anomalies for all 42 winters (NOV) and between observations and all ensemble members (others), all within the extratropical northern hemisphere (NH, $\geq 30^oN$). In the upper two panels the pattern correlations with CLIM-NO (1st) and NOV (2nd) are shown for comparison, showing a normal-like distribution with the mean near zero. The lower two panels are the pattern correlations for the two relaxation experiments CLIM-STRAT (3rd) with the mean slightly shifted to positive correlations and CLIM-TROP20 (4th) with the clearest improvement. The average pattern correlations of the ensemble members for all experiments are given in Table 4.1.*

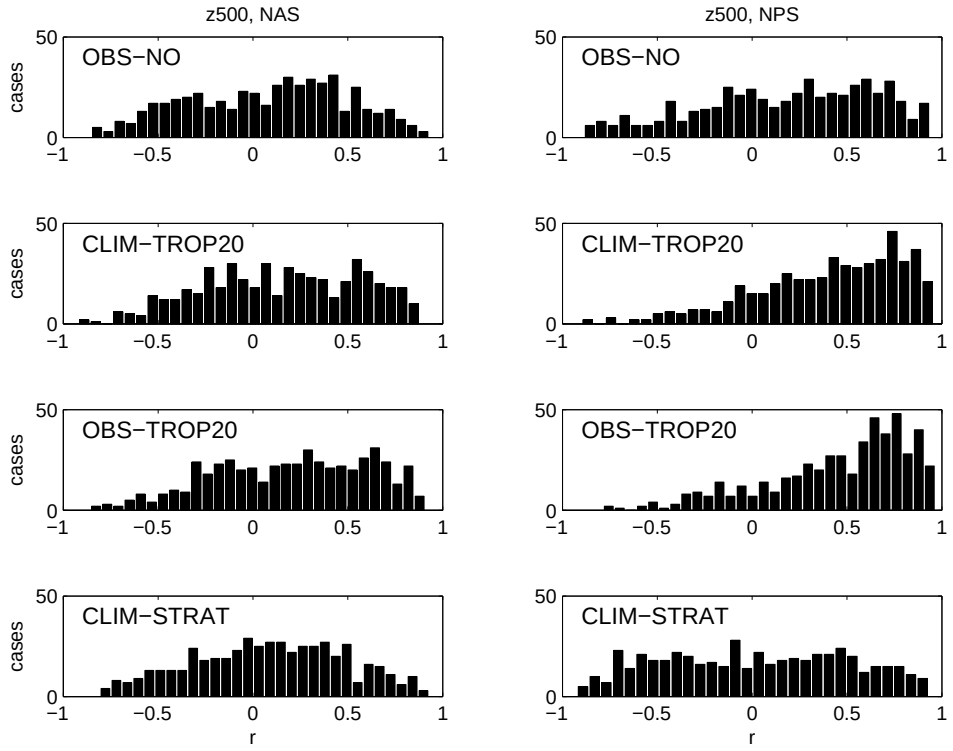

Figure 4.4: *Pattern correlation histograms for the North Atlantic sector (NAS, $30°N - 80°N$ and $90°W - 40°E$, left column), the North Pacific sector (NPS, $30°N - 65°N$ and $160°E - 140°W$, right column) and for the experiments OBS-NO (1st row), CLIM-TROP20 (2nd row), OBS-TROP20 (3rd row) and CLIM-STRAT (4th row). The mean pattern correlations for all experiments are given in Table 4.1. A strong impact of the tropical relaxation can be seen for the NPS, while in the NAS the impact of tropical and stratospheric relaxation are less obvious, but still visible.*

Table 4.1: *Average pattern correlations $\overline{\rho_{pc}}$ between single model realisations (single years for NOV) and observations at Z500. Values are given for the extratropical northern hemisphere (NH), the North Atlantic sector (NAS) and the North Pacific sector (NPS). The values noted here are also the means of the corresponding distributions shown in Figures 4.3 and 4.4.*

Experiment	NH	NAS	NPS
CLIM-NO	-0.01	-0.04	-0.02
NOV	0.02	< 0.01	0.03
OBS-NO	0.11	0.08	0.18
CLIM-TROP20	0.24	0.15	0.40
OBS-TROP20	0.29	0.20	0.45
CLIM-STRAT	0.06	0.08	0.01

Table 4.2: *The probability of positive pattern correlations between all single ensemble members from each experiment for all years in percent (100% correspond to 504). The pattern correlations are computed for $500hPa$ height anomalies as for Figures 4.3 and 4.4. The number of positive correlations for the model experiments is therefore divided by $12 \times 42 = 504$ and by 42 for the NOV experiment.*

Experiment	NH	NAS	NPS
CLIM-NO	49	46	48
NOV	52	48	50
OBS-NO	66	60	65
CLIM-TROP20	83	63	84
OBS-TROP20	86	67	86
CLIM-STRAT	56	58	51

correlated to the observations than CLIM-STRAT ($\overline{\rho_{pc}} = 0.08$).

Globally prescribed observed SSTSI in OBS-NO lead to slightly higher pattern correlations in the NH, and especially the NPS, where the average spatial correlation between ensemble members and observations is $\overline{\rho_{pc}} = 0.12$ and $\overline{\rho_{pc}} = 0.18$ respectively (see Table 4.1). In the NAS the average pattern correlations are only slightly shifted away from zero $\overline{\rho_{pc}} = 0.08$. The probability of positive correlations is larger than 60% in the NH, NAS and NPS (Table 4.2). This means that except for the NAS, OBS-NO yields better results than the relaxation experiment CLIM-STRAT.

4.1.1 Analysis of NAO indices

In Figure 4.5 the NAO indices from the different experiments are shown for Z500 as an example for the tropospheric circulation. The indices for the model experiments are obtained by projection of the model anomaly fields onto the NAO pattern obtained from the EOF analysis of observations within the NAS as introduced in Section 2.3 (see also the figure caption).

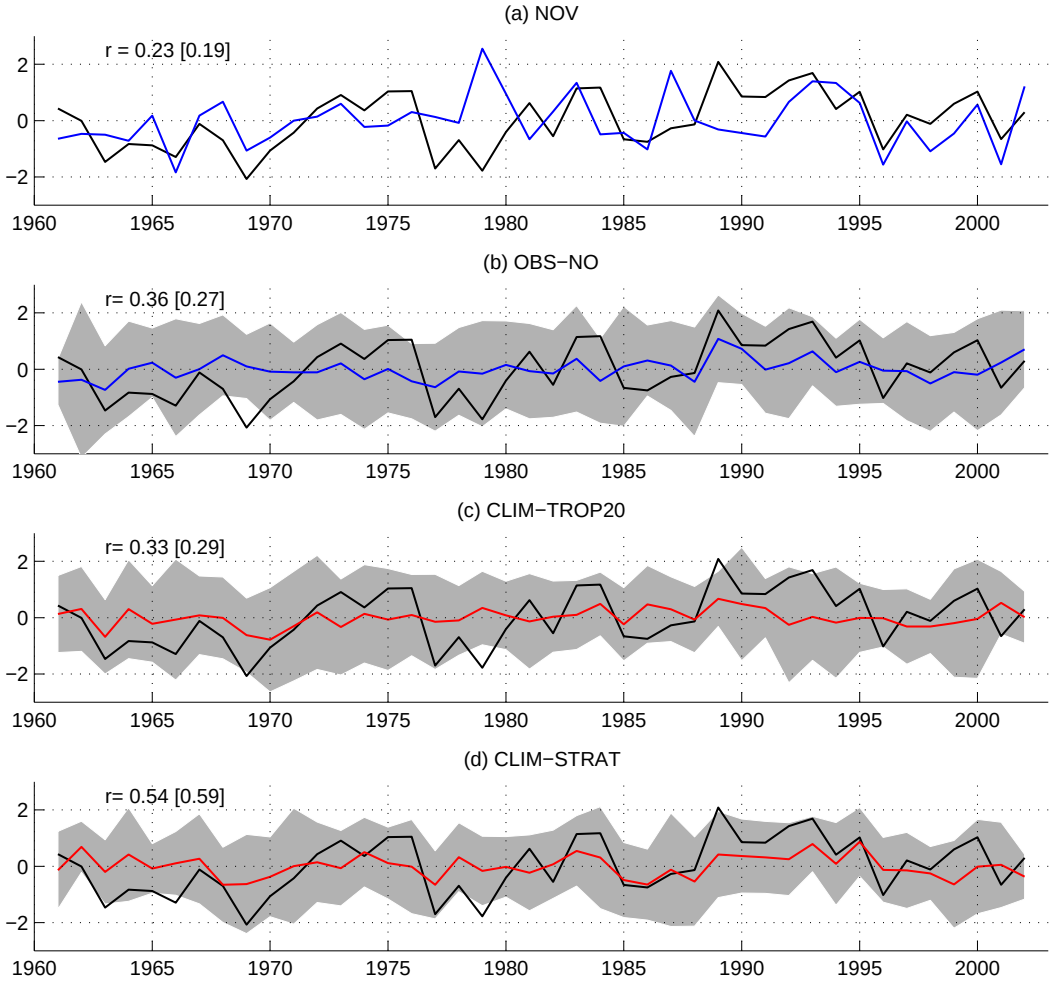

Figure 4.5: *NAO indices for* $500hPa$ *height anomalies. The observed NAO index (black) is the first PC of an EOF analysis of* $500hPa$ *geopotential height anomalies in the NAS* $(30°N - 80°N,\ 90°W - 40°E)$*. All other indices are obtained by projection of model anomalies onto the NAO pattern corresponding to the observed NAO index.*
Blue (red) indices are ensemble means without (with) relaxation. The grey shading indicates plus/minus 1 and 2 standard deviations of the ensemble members, deviating from the ensemble mean. Straight lines are the linear trends corresponding to the index of the same colour. Correlation of the (detrended) ensemble mean indices with the (detrended) observed index is given in the figure in brackets.

Table 4.3: *Interannual correlation coefficients between observed NAO index for SLP and Z500 (NAM index for Z50 and Z10) and corresponding ensemble mean index from 12 ensemble members. Correlations for detrended indices in brackets. One (Two) asterisk marks correlations exeeding* 0.31 *(*0.40*) which are different from zero at a* 95% *(*99%*) level. By doing Monte Carlo simulations we find that the significance levels are the same for all experiments (see Figure 4.6).*

Experiment	SLP	Z500	Z50	Z10
CLIM-NO	-0.36* [-0.29]	-0.35* [-0.29]	0.03 [0.06]	0.20 [0.20]
NOV	0.25 [0.20]	0.23 [0.19]	0.34* [0.33*]	0.21 [0.22]
OBS-NO	0.45** [0.35*]	0.36* [0.27]	0.32* [0.32*]	0.16 [0.16]
CLIM-TROP20	0.36* [0.29]	0.33* [0.29]	0.46** [0.49**]	0.42** [0.43**]
CLIM-TROP10		0.29 [0.24]		
OBS-TROP20	0.50** [0.38*]	0.45** [0.37*]	0.60** [0.63**]	0.57** [0.58**]
CLIM-STRAT	0.54** [0.59**]	0.54** [0.59**]		

Table 4.4: *Mean standard deviation* $\overline{\sigma}$ *of the NAO (NAM for Z50 and Z10) index values from all ensemble members about the ensemble mean of each experiment over the entire period. Comparison with the correlation values in Table 4.3 shows that the spread amongst the ensemble members is smallest when the correlation is highest.*

Experiment	SLP	Z500	Z50	Z10
CLIM-NO	0.80	0.85	0.82	0.69
OBS-NO	0.75	0.80	0.77	0.65
CLIM-TROP20	0.71	0.74	0.75	0.66
OBS-TROP20	0.69	0.71	0.73	0.62
CLIM-STRAT	0.64	0.67		

Each NAO index is normalised by the standard deviation of the observed NAO index. The ensemble mean index is obtained as the average of the 12 index values of the ensemble members in each year. Calculating the ensemble mean eliminates the atmospheric noise or internal variability in the atmosphere, so that the mean shows the forced signal of each experiment. The mean of any index is zero, as the sum over all years at each grid point of each anomaly field is zero after subtracting the climatological mean. Colored indices correspond to the ensemble means and the black ones to the observations. The correlation between the ensemble mean NAO index and the observed NAO index is given in the figure while the correlation between the corresponding detrended time series is given in brackets, showing the effective interannual correlation (see Table 4.3 for the significance of each correlation).

Monte Carlo simulations are done to investigate the significance of the correlations obtained corresponding to Case 1 in Section 3.5. The resulting PDFs of interannual correlations for selected experiments are shown in Figure 4.6. These PDFs are all centered around zero. The 95% and 99% ranges

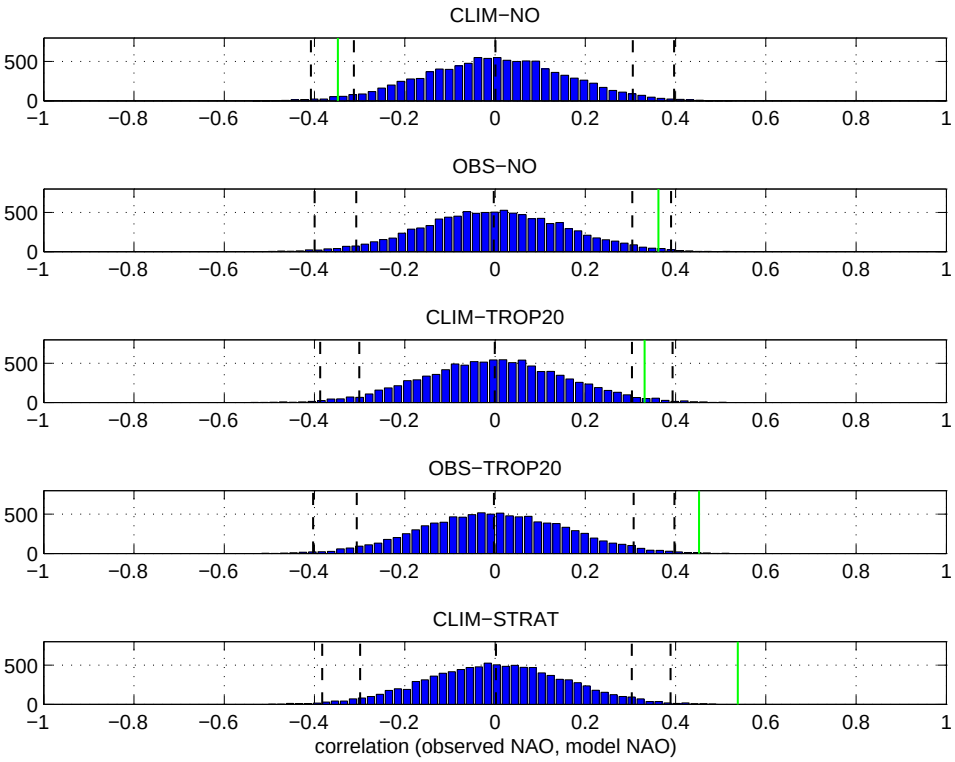

Figure 4.6: *The histograms of correlations between the artificial ensemble mean NAO indices generated by the Monte Carlo method* (10,000 *indices; Case 1 in Section 3.5) and the observed NAO index at* $500hPa$ *(blue bars). Black dashed lines indicate the median as well as the 95% and the 99% ranges of the distribution, the boundaries being used as the significance levels of the correlations. All correlations of the original ensemble means shown here (green lines) are significant. Also compare with Figure 4.11 which shows that the significance levels are the same also for the correlations between PNA indices.*

Table 4.5: *Number of years (out of 42) when the NAO (NAM in the stratosphere) forecast of the ensemble mean has the correct sign. Values are given for all experiments and for our standard quantities. The percentage of winters with a correct ensemble mean forecast of the sign of the NAO is given in brackets. Largest values are bold.*

Experiment	SLP	Z500	Z50	Z10
CLIM-NO	15 (36%)	18 (43%)	21 (50%)	23 (55%)
NOV	22 (52%)	23 (55%)	27 (64%)	26 (62%)
OBS-NO	25 (60%)	21 (50%)	26 (62%)	23 (55%)
CLIM-TROP20	25 (60%)	24 (57%)	**30 (71%)**	30 (71%)
OBS-TROP20	25 (60%)	25 (60%)	29 (69%)	**31 (74%)**
CLIM-STRAT	**28 (67%)**	**26 (61%)**		

Table 4.6: *The same but for the ensemble members*

Experiment	SLP	Z500	Z50	Z10
CLIM-NO	227 (45%)	236 (47%)	256 (51%)	269 (53%)
OBS-NO	275 (55%)	264 (52%)	274 (54%)	266 (53%)
CLIM-TROP20	273 (54%)	274 (54%)	287 (57%)	299 (59%)
OBS-TROP20	**289 (57%)**	273 (55%)	**305 (61%)**	**321 (64%)**
CLIM-STRAT	286 (57%)	**292 (58%)**		

as well as the medians of the distributions are calculated and given in the figure. For example, the 99% range is obtained by calculating the 0.5% and 99.5% percentiles as boundaries so that 99% of the values sit within those boundaries. It can be seen that the thresholds do not differ substantially for the different experiments and we can determine the 95% (99%) significance level at a correlation of $\rho_{95} = 0.31$ ($\rho_{99} = 0.40$) for the following discussion (cf., Figure 4.11: same results for the PNA). Also the November persistence experiment NOV has been tested by shuffling the years and the same result was obtained. The term "significant at x%" is used to indicate that the correlation falls outside the x% range in our discussion, if not differently specified. The results agree with a Students t-test if 42 degrees of freedom are assumed for the test.

The grey shadings in Figure 4.5 mark two standard deviations (STDs) of the ensemble members from the ensemble mean and therefore represent the spread amongst them. In Table 4.3 the interannual correlations for the ensemble means for all heights and all experiments are summarised including their significance while in Table 4.4 the mean STDs for the variability amongst the ensemble members about the ensemble mean over all years is noted as an indication of the spread. Table 4.5 shows the number and the percentage of years in which the ensemble mean NAO index has the correct sign and Table 4.6 likewise for single realisations.

In Figure 4.7 the results from Monte Carlo simulations corresponding to Case 3 on page 26 in Section 3.5 are presented. 10,000 single realisations

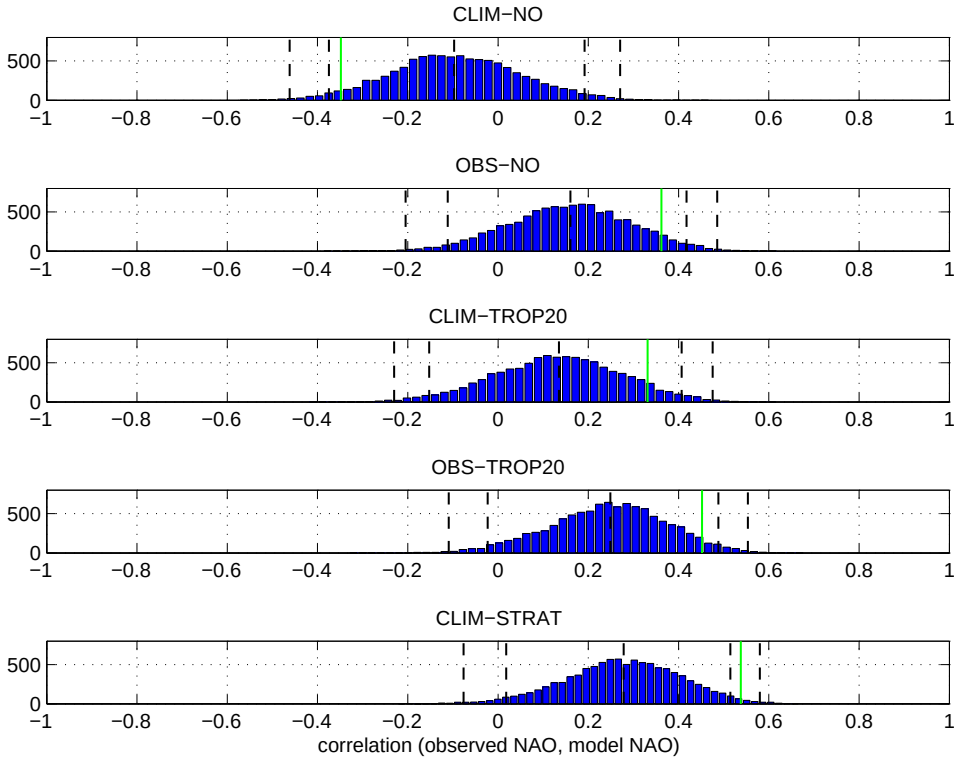

Figure 4.7: *The histograms of correlations between the NAO indices of* $10,000$ *possible realisations and the observed NAO index at* $500hPa$ *(blue bars) none of which was detrended. In contrast to the derivation of the significance levels used to produce Figure 4.6 the years are kept here during shuffling and correlations are calculated for the NAO index of single realisations and the observed NAO index (see Case 3 in Section 3.5). Black dashed lines indicate the median as well as the 95% and the 99% ranges of the distribution. Green line is the correlation of the ensemble mean.*

of the NAO index are generated whilst keeping the years of each value fixed corresponding to possible realisations of the atmosphere of the model in each winter. The PDF of correlations between the model NAO index and the observed NAO index is shown. The strength of the forcings can be seen in the displacement of the center of the PDF from zero.

In the first panel (a) of Figure 4.5 the November anomaly persistence "experiment" (NOV) is compared with the observed NAO index. The correlation with the observed NAO index of $\rho = 0.23$ is not significant at the 95% level even though in some years and periods the persistence of November anomalies resembles well the winter mean NAO, for example in the early 1970s or in the mid 1990s. The correlation value for the detrended time series (in brackets) is smaller which indicates that the trend of November NAO values had the same sign as the trend of the winter mean NAO between 1961

and 2002. In Section 4.2 the trends will be further investigated. Only slightly more than 50% of the November persistence NAO forecast values have the right sign (see Tables 4.5 and 4.6), meaning that there is no forecasting skill in this method.

At $500hPa$ the ensemble mean of OBS-NO (Figure 4.5, (b)) is significantly correlated with the observed NAO index ($\rho = 0.36$) at the 95% level only if the time series are not detrended. The effective interannual correlation is not significant ($\rho = 0.27$). However, the observations are always within the spread (2 STD) of the ensemble members and so are a possible realisation in the experimental setup. These results are similar for the tropical relaxation ensemble CLIM-TROP20 ((c), $\rho = 0.29$ for the detrended time series). At SLP the correlations are higher for OBS-NO and CLIM-TROP20 and are still significant if the time series are detrended (see Table 4.3). The ratio of a correct forecast of the sign of the NAO is slightly higher for CLIM-TROP20 than for OBS-NO at both SLP and Z500 (52% to 62%, see Tables 4.5 and 4.6). In Figure 4.7, the PDFs for correlations between the NAO index of single realisations and the observed NAO index for OBS-NO and CLIM-TROP20 are both centered around a value of slightly smaller than $\rho = 0.2$ which is a lower correlation than that of the ensemble mean. This is in agreement with Bretherton and Battisti (2000) who state that the ensemble mean of a model experiment with a forcing obtained from observations will always have a larger correlation with the observations than its single members (as can be seen for all experiments). It follows that on the basis of the analysis so far, knowledge of global SSTSI for any given winter is roughly equivalent to having a perfect knowledge of the tropics for determining the winter mean NAO index. This means also, however, that the distinct influences of the tropics and SSTSI, if seen over all 42 winters, are not particularly strong.

The ensemble OBS-TROP20 (shown in Figure 4.6 and Table 4.3) shows the combined effect of relaxing the tropics and prescribing extratropical SSTSI. The interannual correlation of its ensemble mean with the observed NAO index is significant at 95% ($\rho = 0.37$) which is higher than that of CLIM-TROP20 but also lower than that of CLIM-STRAT. Also in single realisations (Figure 4.7) both forcings add to each other in OBS-TROP20, resulting in an average correlation, between the NAO index obtained from single realisations and the observed NAO index, of slightly less than 0.3. Prescribing a known evolution of extratropical SSTSI therefore adds skill to the forecast of the NAO index compared to CLIM-TROP20 in which the tropics are perfectly forecasted. This is also reflected by the fact that there are only very few negative correlation values for OBS-TROP20 in Figure 4.7. However, the sign of the NAO forecast is not correct in more than 60 % of the years, regarding the ensemble mean (Table 4.5).

The highest interannual correlation is found between the ensemble mean of CLIM-STRAT and the observed NAO index at $500hPa$ (Figure 4.5, (d),

$\rho = 0.59$) which is significant at the 99% level. Even though the spread of this ensemble is smallest in the average, the observed NAO index is always within the spread of the CLIM-STRAT ensemble members in Figure 4.5. In about two third of the years, the ensemble mean NAO forecast of CLIM-STRAT at SLP has the same sign as the observed NAO index (Table 4.5). The average correlations between single realisations and the observations (shown in Figure 4.7) for this experiment are around $\rho = 0.3$, slightly higher than those of OBS-TROP20. This indicates that the stratospheric forcing for the NAO is slightly stronger compared to that of OBS-TROP20 (tropical forcing + extratropical SSTSI). This is also visible in Figure 4.7, as the PDF for CLIM-STRAT is the narrowest of all experiments and very few single correlations are negative or near zero which means they are very unlikely. The stratospheric relaxation therefore still has the largest impact on the variability of the NAO compared to the other forcings. This confirms the expectation of Scaife et al. (2005) that interannual variations of the NAO are reproduced if the stratosphere is relaxed toward observations.

It is noticeable that in general the average spread in the NAO index of the realisations in one year is smaller the higher the correlation with the observed index is. OBS-NO is an exception with higher correlation than for example CLIM-TROP20 but with a larger spread. The large spread in these cases may be connected to the fact that in these experiments no relaxation is applied and the atmosphere has more freedom to evaluate.

In the stratosphere, tropical relaxation in CLIM-TROP20 and OBS-TROP20 leads to significant interannual correlations between the ensemble mean NAM index and the observed NAM index which are all significant at the 99% level (Table 4.3, $\rho \approx 0.60$). The correlations for OBS-TROP20 are slightly higher, indicating that SSTSI impact the stratosphere on interannual time scales. Seen as ensemble means, the tropical relaxation experiments manage to correctly forecast the sign of the NAM in 70% to 80% of the 42 years (60%-70% for the single realisations, see Tables 4.5 and 4.6). It has to be kept in mind that the tropical stratosphere is relaxed in CLIM-TROP20 and OBS-TROP20 so that the stratosphere is directly affected in the tropics. The coincidence of a strong impact of the tropical relaxation ensembles on the extratropical stratosphere and the high correlation of the CLIM-STRAT ensemble mean NAO index with the observed NAO index can be a hint that the influence of tropical relaxation on the extratropical troposphere is via the extratropical stratosphere.

The CLIM-NO experiment is the "control" ensemble, which has no external forcing except the climatological seasonal cycle of SST and solar insolation. Therefore, no interannual correlation is expected between NAO indices from this experiment and the observations. Here a negative correlation between the original ensemble mean NAO index and the observed NAO index is found to be significant at the 95% level, but not significant for the effective interannual correlation, i.e. after detrending (Table 4.3, Z500:

$\rho = -0.35[-0.29]$). This is present also in SLP, but there is no such significant correlation for the PNA index or for the stratospheric (NAM) indices for this experiment. In Table 4.4 it can be seen that the average STD is largest for CLIM-NO compared to the other experiments. Furthermore, in Figure 4.7 it can be seen that the average NAO correlations of the single realisations in CLIM-NO are small ($\overline{\rho} \approx -0.1$) compared to that of the original ensemble mean ($\rho = -0.35$). The PDF is very close to being centered around zero correlation.

In Figure 4.8 the correlations between observations and the ensemble mean of CLIM-NO at each gridpoint are shown for $500hPa$ heights for different periods. Only significant correlations are plotted ($|\rho| \geq 0.31$) so that the important features emerge. For the whole period 1960/61 to 2001/02 (panel (a)), some negative correlations can be found over the central Atlantic and northern Africa while a region of positive correlation can be found over the Tibetian plateau. The spatial extent of the significant correlations is only small and the regions where the correlations occur are isolated. The negative correlations which are within the NAS where the NAO index is calculated are the reason for the negative correlation between the CLIM-NO ensemble mean NAO index and the observed NAO index. Similar regions of negative correlations are found in the SLP data (not shown), but it is not possible to find a pattern of negative correlations anywhere else in the NH, and also in the NH-stratosphere. It was also found that after detrending, the significant correlation in the NAS is lost and only some positive correlations over the Asian continent remain (not shown). This is consistent with the fact that after detrending the corresponding NAO time series, the correlation between the CLIM-NO ensemble mean and the observations is not significant any more. Comparing the three subperiods (Figure 4.8, panels (b), (c), (d)) it emerges that the areas of correlations larger than 0.31 are not stationary but rather spotty although there is always some negative correlation within the NAS. Nevertheless, we suggest the correlations are not systematic and that the negative correlation within the NAS during the whole period and also the correlation between the ensemble mean NAO index of CLIM-NO and the observed NAO index is coincidental.

The only feature of CLIM-NO that depends on the year is the initial conditions. The decorrelation time scale in the troposphere is about 10 days, so one would expect a PDF which is exactly centered around zero correlation in Figure 4.7. In the stratosphere though, the memory is longer and the initial conditions could contain the "quasi-biennial oscillation" (QBO). This could in fact impact the mean winter NAO (Boer and Hamilton, 2008, found additional NAO forecast skill due to a known QBO), although this would at first sight cause a positive correlation with the observed NAO. Boer and Hamilton (2008) however stated that AGCMs mostly do not represent the processes that produce the QBO so that the effect of the QBO in the initial conditions in the ECMWF model are hard to be foreseen.

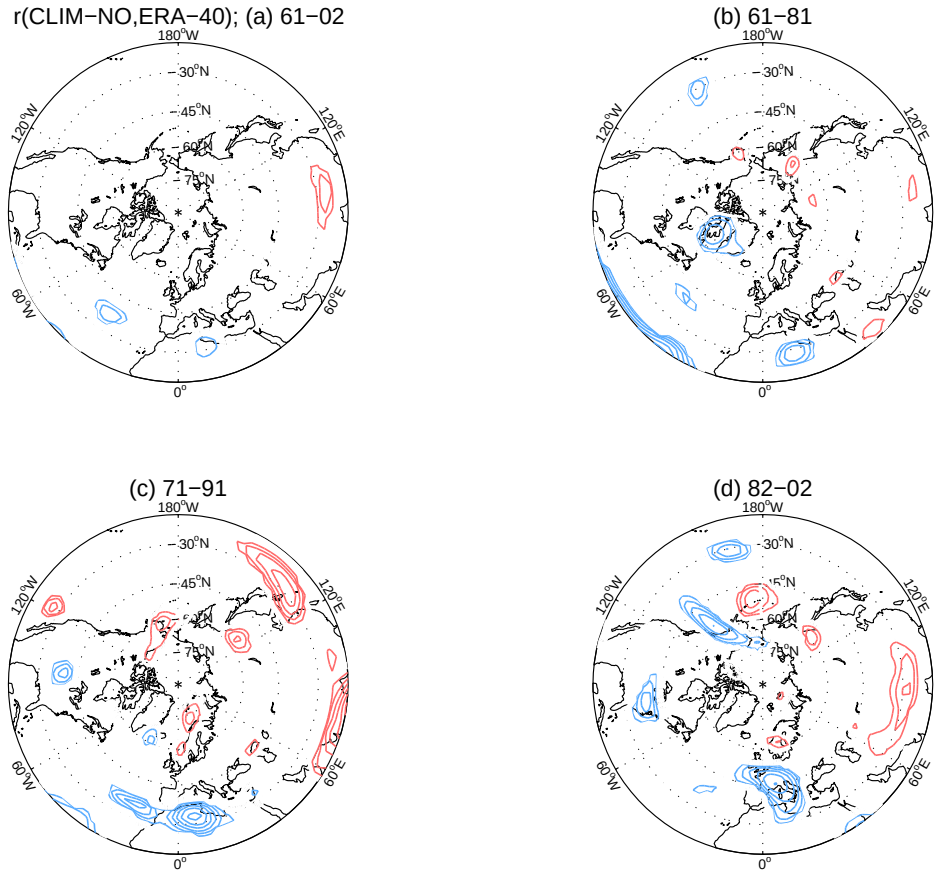

Figure 4.8: *Point correlation r between the evolution of winter mean $500hPa$ geopotential heights of the ensemble mean of CLIM-NO and the reanalysis ERA-40 for the periods: (a) 1960/61 - 2001/02, not detrended; all following are detrended: (b) 1960/61 - 1980/81, (c) 1970/71 - 1990/91 and (d) 1981/82 - 2001/02. Only correlations larger than $|\rho| \geq 0.31$ have been plotted with a contour interval of 0.05 (based on the 95% significance level for 42 years time series obtained from Monte Carlo simulations, see Figure 4.6; note that the significance levels would). The negative correlation over the central Atlantic and northern Africa can be the reason for the negative correlation between the NAO index of CLIM-NO and the observed NAO index.*

Table 4.7: *Like Table 4.3, but for correlations of PNA indices. One (Two) asterisk marks correlations exeeding the 95% (99%) significance levels.*

Experiment	SLP	Z500
CLIM-NO	0.04 [0.04]	0.07 [0.08]
NOV	0.13 [0.12]	0.26 [0.25]
OBS-NO	0.47** [0.48**]	0.53** [0.58**]
CLIM-TROP20	0.80** [0.80**]	0.79** [0.79**]
CLIM-TROP10		0.53 [0.58]
OBS-TROP20	0.78** [0.79**]	0.77** [0.80**]
CLIM-STRAT	0.11 [0.11]	0.04 [0.07]

Table 4.8: *Mean standard deviation $\overline{\sigma}$ of the PNA index values from the ensemble mean for all ensemble members within each experiment over the entire period indicating the spread of the PNA indices between the single ensemble members.*

Experiment	SLP	Z500
CLIM-NO	0.86	0.77
OBS-NO	0.81	0.72
CLIM-TROP20	0.63	0.55
OBS-TROP20	0.61	0.52
CLIM-STRAT	0.83	0.76

4.1.2 Analysis of PNA indices

Figure 4.9 shows the PNA ensemble mean indices of selected experiments compared to the observed PNA index at $500hPa$, similar to Figure 4.5 for the NAO (see figure caption and Section 2.4 for details of the definition of the PNA index). The grey shading again denotes two standard deviations of the ensemble members of the ensemble mean. Additionally to the latter figure, El Niño winters are marked with green circles on the observed PNA index time series. Table 4.7 summarizes the interannual correlations between the ensemble mean PNA indices and the observed PNA index and Table 4.8 summarizes the spread (i.e., the average STD) of the ensemble members about the ensemble mean respectively. In Figure 4.10 the Monte Carlo PDFs of correlations between the single realisations of the PNA index (Case 3, Section 3.5) and the observed PNA index are shown. Tables 4.9 and 4.10 give the number and the fraction of PNA forecasts with a correct sign for all ensemble means and single realisations of the experiments. The significance levels of the correlations are obtained the same way as for the NAO indices so that a correlation of $\rho_{95} = 0.31$ ($\rho_{99} = 0.40$) corresponds to the 95% (99%) significance levels (see Figure 4.11).

The PNA indices obtained from CLIM-NO have no correlation with the observed PNA index in the average and also have the largest spread compared to the other experiments. The ensemble mean PNA index of CLIM-

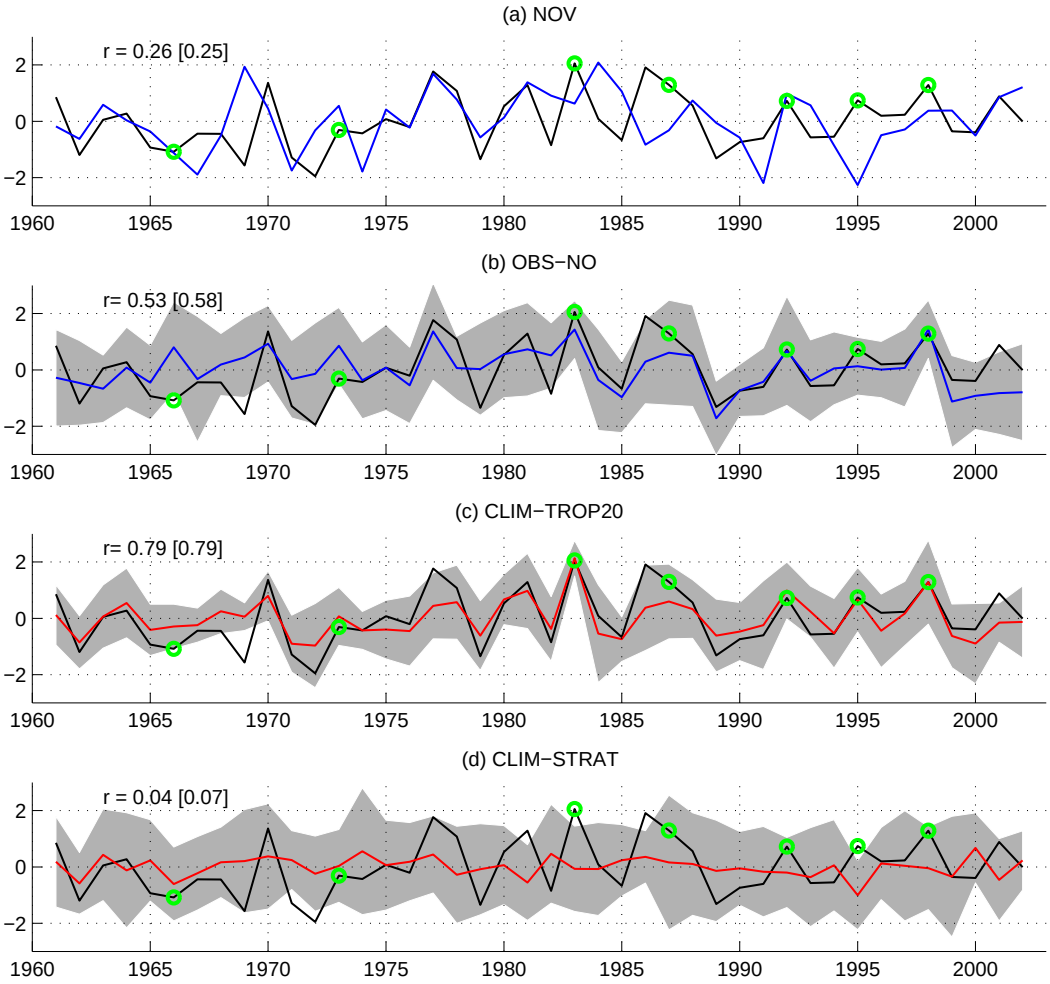

Figure 4.9: *Like Figure 4.5 but for the PNA index (black) at* $500hPa$*. The PNA index for observations is obtained as the weighted area mean of* $500hPa$ *geopotential heights from* $30°N - 65°N$ *and* $160°E - 140°W$*. Green circles mark positive El Niño years (*$\geq 1STD$ *of DJF mean Nino 3.4 SST index as in Figure 2.8).*

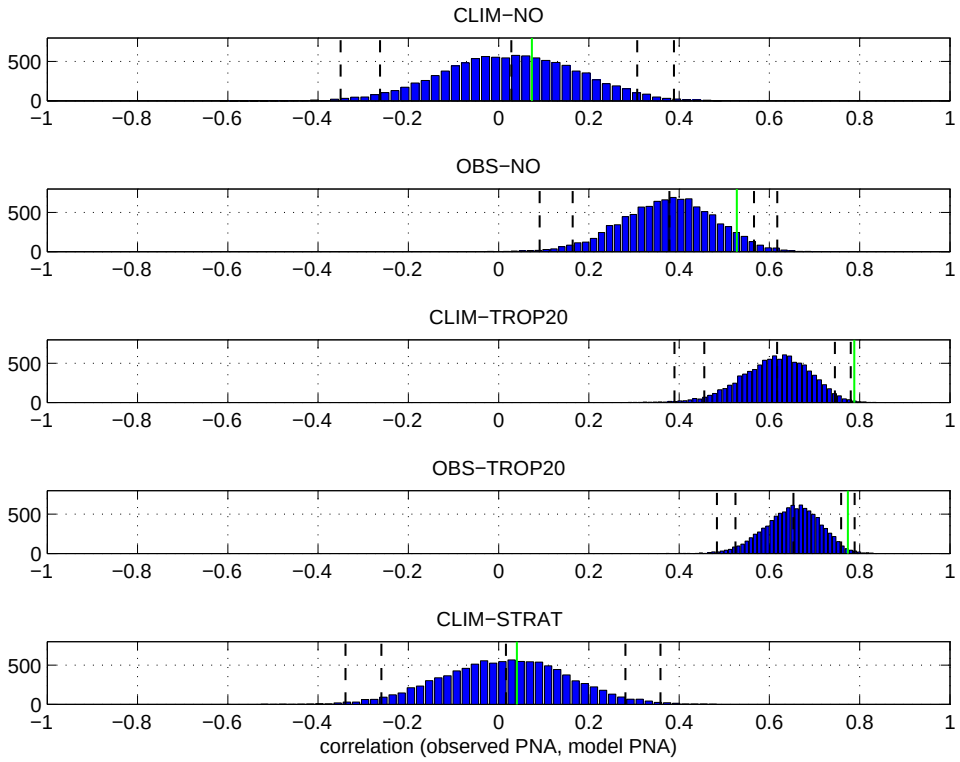

Figure 4.10: *Like Figure 4.7, but for correlations between the PNA indices of observations and ensemble members at 500hPa none of which was detrended. It can be seen that the astonishingly high correlations between the ensemble mean PNA index of CLIM-TROP and OBS-TROP20 are supported by the fact that the PDFs of correlations are far away from zero correlation which appears to be impossible if tropical relaxation is applied. CLIM-STRAT however yields a PDF similar to that of CLIM-NO meaning that the stratospheric is unimportant for the PNA.*

Table 4.9: *Number of years (out of 42) when the PNA forecast, based on the ensemble mean, has the correct sign. The percentage of winters with a correct forecast of the sign of the PNA is given in brackets. Values are given for all experiments and for our standard quantities. Largest values are bold.*

Experiment	SLP	Z500
CLIM-NO	22 (52%)	22 (52%)
NOV	24 (57%)	29 (69%)
OBS-NO	32 (76%)	31 (74%)
CLIM-TROP20	**38 (91%)**	**34 (81%)**
OBS-TROP20	36 (86%)	33 (79%)
CLIM-STRAT	23 (55%)	21 (50%)

Table 4.10: *The same but for the ensemble members*

Experiment	SLP	Z500
CLIM-NO	254 (50%)	247 (49%)
OBS-NO	316 (63%)	320 (63%)
CLIM-TROP20	**387** (77%)	**364 (72%)**
OBS-TROP20	373 (74%)	360 (71%)
CLIM-STRAT	257 (51%)	236 (47%)

NO has no correlation with the observed PNA index ($\rho = 0.07$). Consistently, the PDF of correlations of shuffled PNA realisations (Figure 4.10) is centered around zero and has the widest distribution amongst all experiments.

It can be seen that observed SSTSI in OBS-NO at the lower boundary leads to a significant interannual correlation between the ensemble mean PNA index and the observed PNA index ($\rho = 0.53$, at 99% level). This is caused mainly by the last third of the period ($\rho_{\geq 1988} = 0.76$), in the first third there is only little correlation ($\rho_{\leq 1975} = 0.19$). The spread of the ensemble members is smaller than that of the CLIM-NO experiment and about two third of the PNA forecasts of OBS-NO have the right sign. For the variability of the PNA, prescribing SST is very influential, an influence which is probably via the atmospheric bridge (Alexander et al., 2002).

The tropical relaxation ensemble CLIM-TROP20 produces winter mean PNA values which are highly correlated with the observed PNA index at the 99% level ($\rho = 0.79$). The correlation is high over the whole period and in years of El Niño events the agreement between the ensemble mean of CLIM-TROP20 and the observed PNA index is astonishingly high (except for the 1965/1966 and 1986/1987 El Niños). Also analysing SLP, the correlation between the observed PNA index and ensemble mean index is very high ($\rho = 0.80$). The results are not particular sensitive to a slight change of the relaxation region, as the correlations are still significant for the CLIM-TROP10 experiment ($\rho = 0.53$). It has to be kept in mind that in the CLIM-TROP10 ensemble only 4 members were executed which is not

sufficient to completely average out the atmospheric noise. Additionally the spread amongst the ensemble members is much lower for CLIM-TROP20 than for CLIM-NO, indicating the strong influence of the tropical forcing. The impact of the tropical relaxation for the PNA can be clearly seen in Figure 4.10. Both the PDFs of CLIM-TROP and of OBS-TROP20 realisations are centered around a correlation larger than $\rho = 0.6$ and values smaller than $\rho = 0.4$ are outside the 99% range of both PDFs. It is also evident that extratropical SSTSI add some skill to the tropical relaxation experiment, be it only slightly. This in turn implies that in OBS-NO, the forecasting skill is caused mainly by adding tropical SST. These results are consistent with those of Newman et al. (2003) who note, based on observations, that the PDO is dependent on ENSO on all time scales and that the (oceanic) PDO is directly correlated to the (atmospheric) PNA in winter.

The stratospheric relaxation ensemble CLIM-STRAT does not lead to significant correlations in the Pacific sector. Its ensemble mean PNA index is correlated to the observed one with $\rho = 0.04$ at $500hPa$ ($\rho = 0.11$ in SLP). Also the spread between the members is not really smaller than those of the ensemble without any forcing, CLIM-NO. The weak impact is also visible in Figure 4.10 where the PDF of CLIM-STRAT realisations is nearly identical to that of CLIM-NO except that it is slightly narrower. The results are consistent with the results of the pattern correlation analysis (see Figure 4.4 and Table 4.1). The stratospheric relaxation causes a marginal improvement of the pattern correlations in the NPS compared to CLIM-NO. Only the strong kurtosis of the pattern correlations of CLIM-STRAT within the NPS in Figure 4.4 cannot be retrieved in the analysis of the PNA indices.

It can be seen that detrending of the time series does not influence the significance of the correlations associated to the PNA, in contrast to the results for the NAO described in the previous section. This is in the first place due to the fact that the correlations are more pronounced (no correlation for CLIM-NO and CLIM-STRAT, high correlations for OBS-NO, CLIM-TROP and OBS-TROP20), but also because the trend of the PNA index during the period 1960/61 to 2001/02 is less strong than that of the NAO during the same period (see Section 4.2).

The tropical atmosphere and the evolution of tropical SST, both probably mainly in the Pacific region, have the largest impact on the interannual variability of the PNA. A better forecast of the tropics would thus enhance the seasonal predictability of anomalous winter mean circulations in the extratropical troposphere in the NPS.

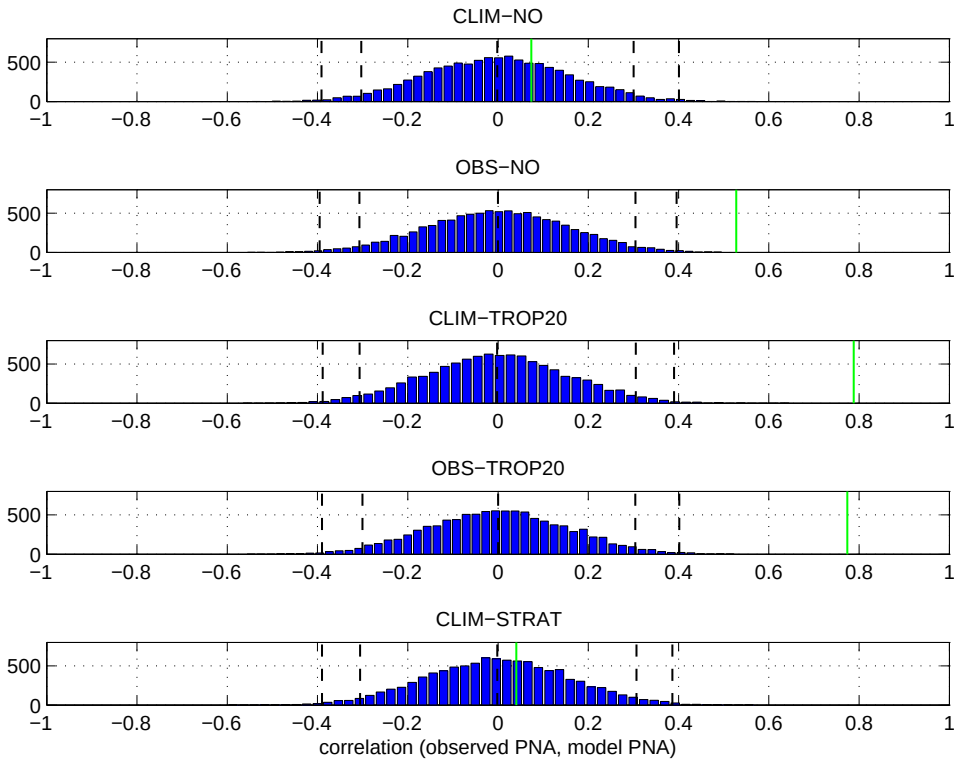

Figure 4.11: *Like Figure 4.6, but for correlations of PNA indices at* $500hPa$*. The significance levels are approximately the same for all experiments and also the same as for the NAO.*

4.2 Trends during the ERA-40 period

As mentioned in Chapter 2, a climate regime shift was detected during the late 1970s in the Pacific sector (Trenberth et al., 2002), changing the variability of teleconnection patterns like the PNA (Greatbatch et al., 2004). On the other hand, the NAO index went through a positive trend from the early 1970s to the mid 1990s and there is disagreement about the origins of this trend in model simulations. It is consistent with being generated just by chance due to internal variability of the coupled climate system (Semenov et al., 2008). Also changing conditions in single components of the system could be the reason, e.g. in the tropics (Lu et al., 2004), in the stratosphere (Scaife et al., 2005), as well as in low frequency ocean dynamics. Here, possible origins of trends in the winter NAO and PNA indices are investigated using the relaxation experiments described in Section 2.2.1.

As a first step, the patterns of the ensemble mean trends in $500hPa$ geopotential heights are compared to the observed one in Figure 4.12. The observed linear trend in $500hPa$ in winters from 1961 to 2002 exhibits deepenings of the Icelandic ($\approx -20m/10yr$) and the Aleutian ($\approx -20m/10yr$) troughs, deepening geopotential over Russia ($\approx -15m/10yr$) and rising geopotential heights over East Asia ($\approx +5m/10yr$), North America ($\approx +10m/10yr$) and Europe ($\approx +15m/10yr$). The observed trend pattern strongly projects on to the NAO and the PNA patterns respectively, so that it is reasonable to investigate the trends of the respective indices in the following sections. The amplitudes of the trends are slightly stronger than found for the period 1949 to 1999 by Lu et al. (2004). Lu et al. (2004) noted that the pattern of the trend is similar to the "Cold Ocean Warm Land" (COWL) pattern of Wallace et al. (1995). The trend pattern looks similar for SLP (not shown).

The ensemble mean linear trends from our model experiments have a smaller amplitude compared to the observations. Hence, the contour interval for the ensemble mean trends in Figure 4.12 is reduced by 1/4 compared to the observations to allow for a comparison of the patterns. OBS-NO, CLIM-TROP20 and OBS-TROP20 reveal similar trend patterns to that observed in our period. OBS-NO has the wrong trend sign in the NPS so that despite a very good accordance in the NAS, the trend pattern correlation over the NH north of 30^oN is only $\rho_{pc} = 0.36$. The trend of CLIM-TROP20 is higher correlated overall to the observed trend ($\rho_{pc} = 0.41$) and only fails to represent the trend over North America and Central Asia. The best accordance can be found for the OBS-TROP20 ensemble ($\rho_{pc} = 0.63$) which yields weak deficiencies only over the Asian continent. These results are similar to that of Lu et al. (2004) who used a simple dynamical model to examine the influence of trends in the tropics on extratropical tropospheric circulation trends.

There is no accordance of trends between the ensemble mean of CLIM-

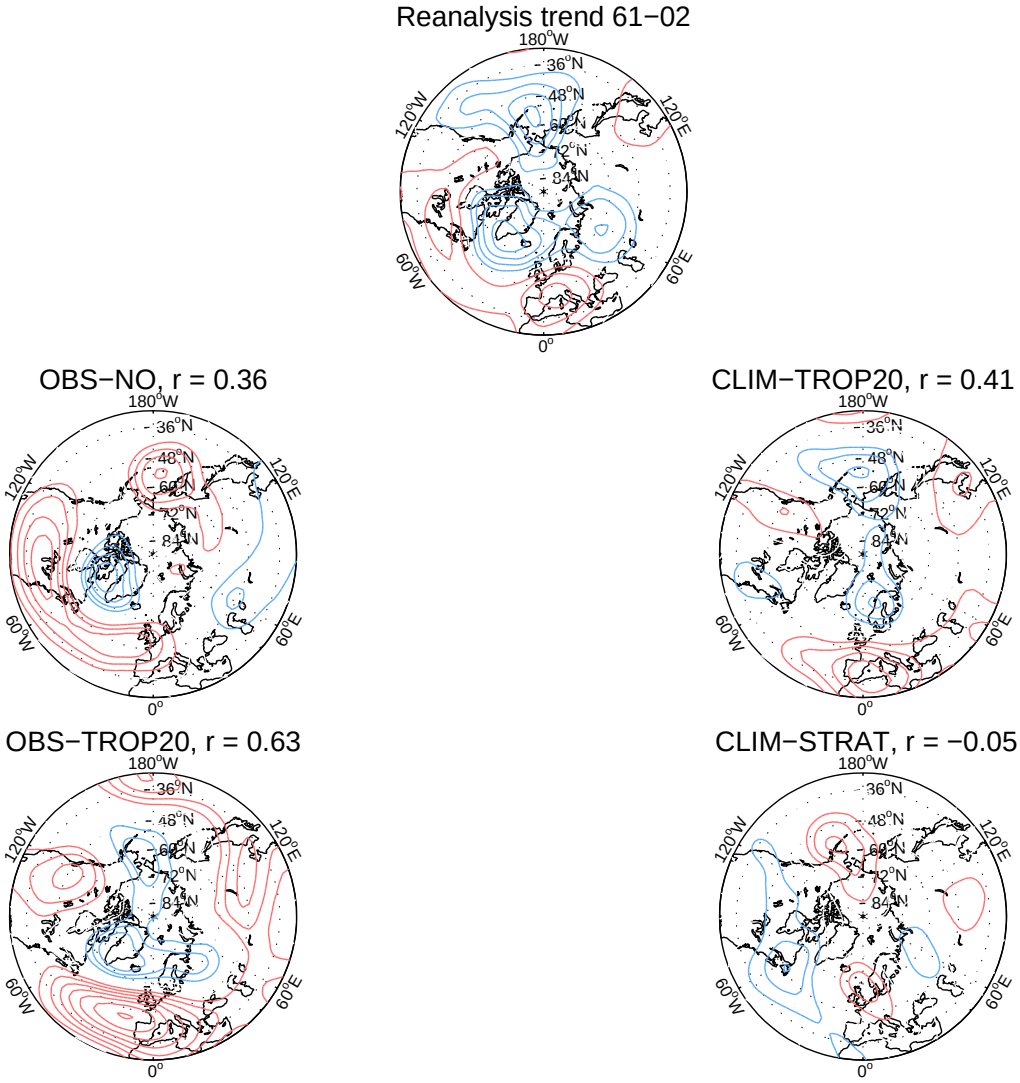

Figure 4.12: *Linear trends of* $500hPa$ *geopotential heights in observations (top) and ensemble means (middle and bottom) in the extratropical NH (north of* 30^oN*) for winters from 1961 to 2002. Red denotes positive trends and blue negative trends in geopotential heights, while the contour interval is* $5m/10yr$ *for the observed trend and* $1.25m/10yr$ *for the ensemble mean trends; the zero contour line is omitted. The pattern correlations* r *with the observed trend pattern north of* 30^oN *are given above the plots.*

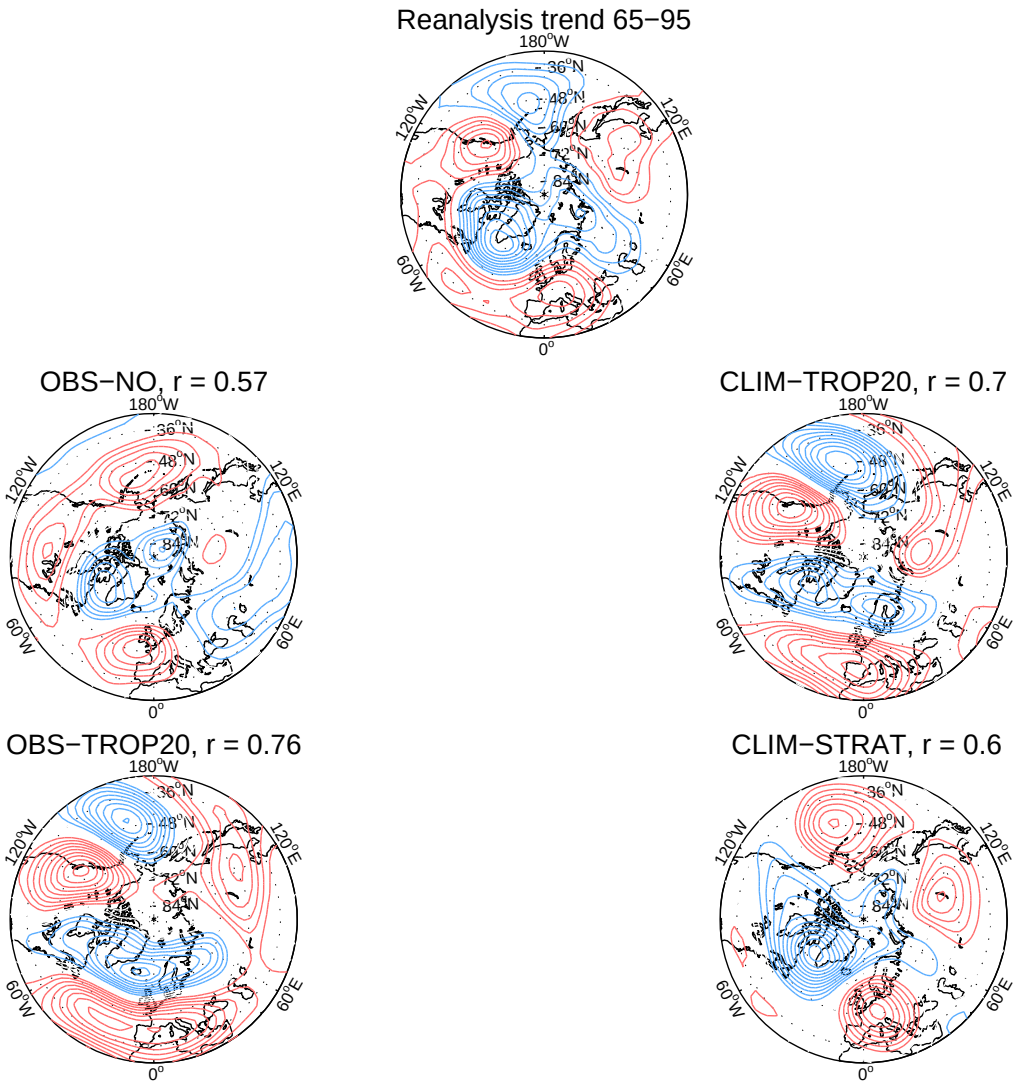

Figure 4.13: *Like Figure 4.12, but for the sub-period 1964/65 to 1994/95. Red denotes positive trends and blue negative trends in geopotential heights, while the contour interval is* $5m/10yr$ *for observed trend and* $1.25m/10yr$ *for the ensemble mean trends; the zero contour line is omitted.*

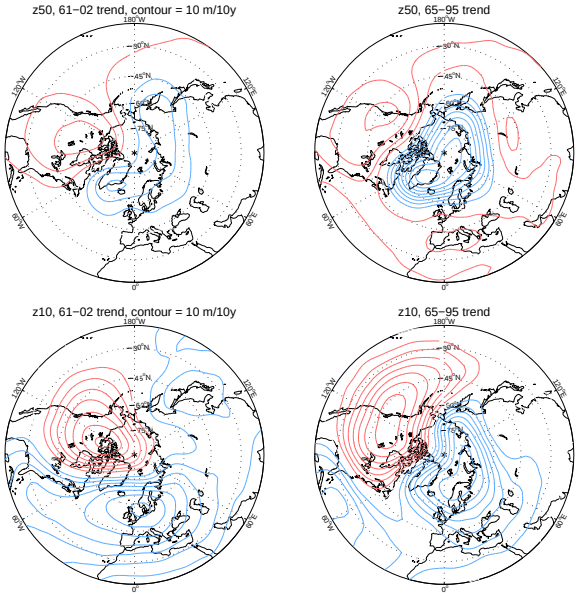

Figure 4.14: *The observed trends in mean winter geopotential heights in the stratosphere. Contour interval is m/yr while red means positive and blue negative while the zero contour line is omitted. First row shows the trends at $50hPa$ and second the trends at $10hPa$. First column gives the trend between 1961 and 2002 while second column gives the trend between 1965 and 1995.*

STRAT and the observations ($\rho_{pc} = -0.05$) in the NH; in the NPS the trend pattern is even of the opposite sign compared to the observed trend. This is in contrast to the results of Scaife et al. (2005) who used a different forcing method to investigate the stratospheric influence on the tropospheric decadal trends between 1965 and 1995 and found a strong impact on the 30-year trend in the NAS in SLP. If we analyse our results during the sub-period between 1965 and 1995 (Figure 4.13), we also find a very strong impact of the stratospheric relaxation in the NAS which strongly projects onto the NAO. The trend pattern correlation changes from -0.05 (1960/61 to 2001/02) to 0.64 (1964/65 to 1994/95) for CLIM-STRAT so that the stratospheric forcing has a similar impact on the hemispheric trend as the other forcings. Our results therefore confirm the findings of Scaife et al. (2005). It is remarkable that the observed trend at Z500 between 1964/65 and 1994/95 was about 50% stronger than between 1960/61 and 2001/02 (identical contour interval in Figures 4.12 and 4.13). In the NPS, OBS-NO and CLIM-STRAT still yield a trend opposite to the observed trend during the sub-period. The ensemble mean of CLIM-NO reveals a trend pattern which is very weak in either of the periods compared with the other ensemble mean trends and negatively correlated to the observed one ($\rho_{pc} = -0.46$, not shown), but the relatively high correlation value is probably spurious.

Table 4.11: *Ratios of ensemble mean NAO/NAM trends and observed ERA-40 NAO/NAM trend over the period 1960/61 to 2001/02. Values closest to 1 are bold. Observed trends are: SLP:* 1.41 $\sigma/42yr$*; Z500:* 1.35 $\sigma/42yr$*; Z50:* 0.30 $\sigma/42yr$*; Z10:* -0.11 $\sigma/42yr$*;*

Experiment	SLP	Z500	Z50	Z10
CLIM-NO	-0.14	-0.13	-1.13	**1.66**
NOV	0.32	0.32	**1.11**	-2.84
OBS-NO	0.32	0.31	0.16	-0.87
CLIM-TROP20	0.21	0.15	-1.13	3.60
OBS-TROP20	**0.49**	**0.40**	-1.02	2.95
CLIM-STRAT	-0.01	>-0.01		

The observed trend in the NH stratosphere was significantly stronger in the sub-period between 1965 and 1995 ($\approx -8m/yr$ at Z50 over the pole, Figure 4.14) than in our whole period 1961 to 2002 ($\approx -3m/yr$ at Z50) when the trend pattern is also much less annular than in the sub-period (Figure 4.14). It is therefore likely that the stratospheric impact on the trends of geopotential heights in the NAS in the period 1965 to 1995 is real. However, it is not possible to conclude from the results in which way the impact took place in reality, but they confirm the strong connection between troposphere and stratosphere in the NAS in winter.

4.2.1 NAO/NAM

The NAO indices shown in Figure 4.5 are investigated regarding their trends. If σ is one standard deviation (STD) of the observed NAO index values, the NAO trend between 1961 and 2002 was $1.33\sigma/42yr$ at $500hPa$ and $1.44\sigma/42yr$ in SLP. The ratios of the ensemble mean trends to the observed trend are given in Table 4.11. In Figure 4.15 the results of the Monte Carlo experiments corresponding to Case 2 on page 25 in Section 3.5 are shown for $500hPa$. It can be examined here if the observed trend can be captured by the model and the different experimental setups.

Consistent with the negative pattern correlation of $\rho = -0.46$ over the whole extratropical NH, it can be seen in Table 4.11 that the "control" CLIM-NO ensemble does not have an NAO trend similar to the observed. The PDF of NAO trends for single realisations is centered around zero and has a very broad range (Figure 4.15), but the observed NAO trend sits outside the 99% range of the PDF. This is in a way contrary to the results of Semenov et al. (2008) who stated that the positive NAO trend between 1965 and 1995 lies within the natural variability of the coupled climate system. They however used a fully coupled model with considerably longer and continuous model runs and looked at slightly different time spans (30 years instead of 42). In the stratosphere at $10hPa$ the ensemble mean CLIM-NO NAM index has a high accordance with the observations showing that the weak negative

observed NAM trend lies within the scope of atmospheric internal variability.

In the North Atlantic sector (NAS) the ensemble mean with tropical relaxation (CLIM-TROP20) reveals a trend pattern projecting onto a positive NAO pattern at $500hPa$ (see Figure 4.12). The center of the negative trend region over Greenland is shifted eastwards compared to the observations, still yielding an NAO trend which has the same sign as the observed one. The CLIM-TROP20 ensemble mean NAO index represents $15-23\%$ of the observed NAO trend (Table 4.11) and the PDF shown in Figure 4.15 for single CLIM-TROP20 realisations is slightly shifted towards the observed NAO trend which however is still outside the 99% range of the PDF.

Historically varying SST and sea-ice (OBS-NO) yield a similar result to that of tropical relaxation in the ensemble mean but with a slightly stronger NAO trend ($\approx 30\%$ of the observed). The observed NAO trend is within the 99% range of the PDF here, which is of a similar width as the PDF of the CLIM-NO realisations, but clearly shifted toward the observed trend. The trend PDFs of realisations are wider for the experiments without relaxation than for those with relaxation indicating that the model atmosphere is less constrained without relaxation. The observed NAO trend is more likely to be captured if the evolution of tropical and extratropical SST is known (OBS-NO). However, the region of the negative trend in the NAS is slightly shifted westward and the region of rising geopotential in the lower latitudes is shifted northward compared to the observations (Figure 4.12).

The ensemble mean NAO index of OBS-TROP20 represents about $40-50\%$ of the linear trend compared to the observed NAO trend, which is also evident in the trend pattern which is very similar to the observed one. The observed NAO trend is within the 99% range of the PDF of trends of that experiment which has a somewhat narrower range than that of OBS-NO. Comparing the PDFs of OBS-NO, CLIM-NO and OBS-TROP20 it is evident that the tropical relaxation has a smaller effect on the NAO trend than the evolution of extratropical SSTSI as the PDFs of OBS-NO and OBS-TROP20 are very similar.

For the period 1961 to 2002, the stratospheric relaxation experiment CLIM-STRAT reveals a small effect of the stratosphere on the NAO trend both in the ensemble mean trend pattern and in the magnitude of the trends of ensemble mean and single realisations. The ensemble mean trend of CLIM-STRAT is near zero and the trend PDF of realisations in Figure 4.15 (left column) is centered around zero with a slightly smaller width compared to that of CLIM-NO. As mentioned in the previous section, this is contrary to the results of Scaife et al. (2005), but if the period of the analysis is restricted to the period between 1965 and 1995 (Figure 4.15, right column), the ensemble mean NAO index of CLIM-STRAT represents about 40% of the observed NAO index and the PDF of trends is shifted toward the observed trend. Accordingly, the PDF of CLIM-STRAT realisations taken from this sub-period has a much smaller width than for the whole period

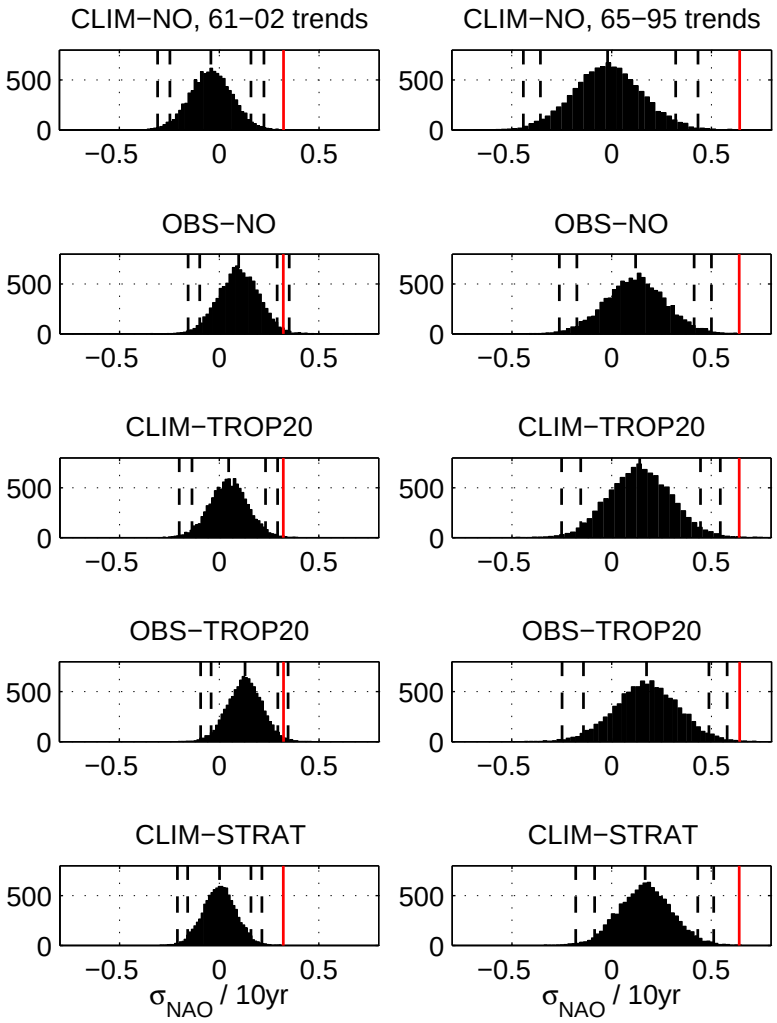

Figure 4.15: *Left column: Histograms of 500hPa NAO trends (in units of standard deviation per 10 years) between 1961 and 2002 in individual model realisations generated as described in Section 3.5. Right column: The same for the 1965 to 1995 sub-period. Red lines show the observed NAO trend. Black dashed lines indicate the median as well as the 95% and the 99% ranges of the distribution.*

Table 4.12: *Ratios of ensemble mean PNA trends and observed ERA-40 PNA trend. Observed trends are: SLP:* 0.48 $\sigma/42yr$*; Z500:* 0.75 $\sigma/42yr$*; Values closest to 1 are bold.*

Experiment	SLP	Z500
CLIM-NO	0.12	-0.05
NOV	**0.70**	**0.40**
OBS-NO	-0.02	-0.49
CLIM-TROP20	0.32	0.20
OBS-TROP20	0.18	-0.13
CLIM-STRAT	-0.04	-0.18

and is even narrower than those PDFs of the tropical relaxation experiments during the sub-period. This indicates that during the 1965-1995 period the stratosphere had a strong impact on the NAO.

Between 1961 and 2002 however, prescribing the evolution of SSTSI (OBS-NO and OBS-TROP) causes trends which have the largest accordance with the observed trends in the NAS or of the NAO trends respectively.

4.2.2 PNA

The overall trend between 1961 and 2002 of the winter PNA was 0.75 $\sigma/42yr$ (0.48 $\sigma/42yr$ at SLP) and is investigated here in the context of the regime shift in the late 1970s. The corresponding ensemble mean indices can be found in Figure 4.9 and the ratios of the ensemble mean trends to the observed trend are shown in Table 4.12 for $500hPa$ and SLP. The following descriptions refers to the results of the analysis of $500hPa$ geopotential heights. In Figure 4.16 the results of the Monte Carlo experiments is shown to examine the unusualness of the observed PNA trend in selected model setups.

For the "control" experiment CLIM-NO we find that the PDF of PNA trends from the Monte Carlo experiments is centered around zero in Figure 4.16, but also that the range of trends of the single members is quite broad. The observed PNA trend therefore lies within the 95% range of trends in the model setup with climatological seasonal cycle of SST and solar forcing. Internal variability of the extratropical atmosphere can thus not be excluded as a reason for the observed PNA trend.

In previous studies, the tropical Pacific and the tropical atmosphere in the Pacific sector were found to influence the PNA on different timescales (e.g. Alexander, 1992). A shift to more frequent occurrence of winters with a warm El Niño event was observed after the late 1970s, suggesting a change of conditions in the tropical Pacific (Trenberth and Hurrell, 1994). Accordingly, our tropical relaxation experiment CLIM-TROP20 produces a trend which, in the ensemble mean, is similar to the observed one in its spatial pattern

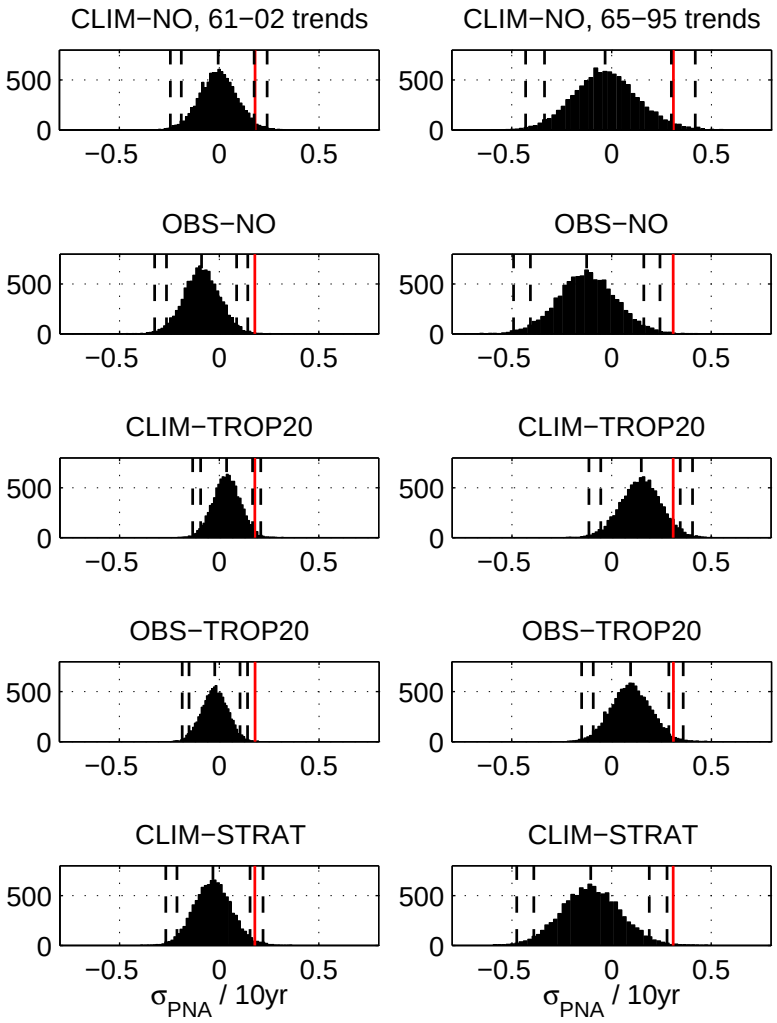

Figure 4.16: *Left column: Histograms of 500hPa PNA trends (in units of standard deviations per 10 years) between 1961 and 2002 in individual model realisations generated as described in Section 3.5. Right column shows the same for the 1965 to 1995 sub-period. Red lines show the observed PNA trend. Black dashed lines indicate the median as well as the 95% and the 99% ranges of the distribution.*

(see Figure 4.12) and in amplitude of $20 - 30\%$ (see Figure 4.16 and Table 4.12). In Figure 4.16 it can be seen that the PDF of trends for CLIM-TROP20 realisations is shifted towards the observed PNA trend compared to the CLIM-NO experiment and the observed trend lies within the 99% range, but slightly outside the 95% range. The origin of the trend of the PNA pattern could therefore be located in the tropics. The wideness of the PDF is small compared to that of CLIM-NO and OBS-NO, indicating a strong influence of the forcing.

The OBS-NO experiment yields a negative ensemble mean PNA trend which can be seen by comparing the sign of the trend in the North Pacific sector in Figure 4.12 and also in Figure 4.16 where the PDF of trends for realisations of this experiment is shifted away from the observed trend compared to the control experiment CLIM-NO. The observed PNA trend is outside the 99% range of the PDF of OBS-NO trends and the ensemble mean PNA trend has an amplitude of -49% of the observed one (see Table 4.12). The PDF of trends has large range, similar to that of CLIM-NO suggesting that the forcing of prescribing observed SST is weak on decadal time scales in the North Pacific sector (NPS) during the period 1961-2002 (the results are similar for the period 1965 to 1995, see Figure 4.16, right column). Copsey et al. (2006) suggest that atmosphere-only models are deficient at correctly representing SLP trends when SSTs are prescribed, for example in the Indian Ocean region. Indeed, the SLP trend of the OBS-NO ensemble mean has, in the Indian Ocean region (30^oE - 100^oE, 35^oN - 35^oS), an opposite average trend of SLP ($-0.005hPa/10yr$) compared to that observed ($+0.5hPa/10yr$). The Indian Ocean has seen a warming trend in our period which has been recognized as a greenhouse gas signal by Hurrell et al. (2004). In the coupled atmosphere-ocean system, conditions of reduced convection and increased solar insolation lead to warm SST anomalies whereas atmosphere-only models run with specified SST tend to generate convection and increased precipitation over warm SST anomalies leading to the opposite behavior in the model from what is observed.

The ensemble members with specified observed global SST combined with tropical relaxation (OBS-TROP20) yield a PDF of linear PNA trends with a negative and weak mean trend (Figure 4.16). It therefore lies in between the PDFs of OBS-NO and CLIM-TROP20 and the wideness of the PDF is small, similar to that of CLIM-TROP20 and the observed PNA trend is outside the 99% range of the PDF. That suggests that prescribing observed extratropical SSTSI degrades the PNA trend.

CLIM-STRAT, the ensemble with stratospheric relaxation as a forcing yields a PDF of PNA trends (Figure 4.16) which looks similar to the PDF of the control experiment CLIM-NO, with the mean near zero and a relatively wide range so that the observed PNA trend is within the 99% range in this case and so is a possible realisation in the context of this experiment. However, this result is not independent of the period of interest in so far

that between 1965 and 1995, the observed PNA trend is outside the 99% range of trends of CLIM-STRAT realisations (Figure 4.16, right column). The ensemble mean PNA trend has an amplitude of −18% of the observed PNA trend indicating that it has the wrong sign. As shown in Figure 4.12, the ensemble mean trend pattern for CLIM-STRAT is quite of the opposite sign compared to the observations in the NPS.

Chapter 5

Conclusions and discussion

In this study, hindcast experiments were analysed to examine the influence of different parts of the climate system on the interannual variability and trends in the winter mean circulation of the extratropical troposphere of the northern hemisphere during the ERA-40 period between 1960/61 and 2001/02. $500hPa$ geopotential heights were mainly used for the analysis. The focus of the analysis of the interannual variability has been on the seasonal predictability skill which could be added by assuming perfect predictability in the region of the added forcing. The added forcing of the model experiments was applied using the relaxation technique (Section 2.2) to constrain the atmosphere toward reanalysis data in different regions, i.e., the tropics or the stratosphere. Also prescribed observed SST and sea-ice (SSTSI) were used as a forcing for the winter circulation and a "control" experiment with the climatological mean cycle of SSTSI and solar forcing was analysed.

In the northern hemisphere (NH) as a whole and the North Atlantic sector (NAS) in particular, tropical relaxation (CLIM-TROP20 and OBS-TROP20) adds most forecast skill in our experiments (Section 4.1, Figures 4.3 and 4.4). The stratosphere (CLIM-STRAT) however has a larger impact on the NAO related part of the tropospheric circulation variability than does the tropical atmosphere (Section 4.1.1). This means that a better representation of the stratosphere, but also the tropical atmosphere, is important for the seasonal forecast of the NAO. It also confirms that the stratosphere is dynamically important for the NAO related variability in the NAS, be it by the downward propagation of stratospheric anomalies or by radiative effects due to greenhouse gases or ozone. It is also possible that part of the NAO forecast skill which is added by relaxing the tropics is dynamically caused by tropical circulation anomalies propagating poleward, affecting extratropical standing waves, for example in the North Pacific sector which in turn impact the polar vortex in the stratosphere that in turn impacts the NAO (Ineson and Scaife (2008) suggested this mechanism). Prescribing global

SSTSI (OBS-NO) leads to a similar amount of NAO related variability compared with the tropical relaxation in CLIM-TROP20. Extratropical SSTSI seem to play a role for the interannual variability of the NAO as the ensemble OBS-TROP20 has a larger skill in capturing the interannual variability than CLIM-TROP (see Section 4.1.1, Table 4.3 and Figure 4.7). The variability of the atmospheric circulation in the North Atlantic sector remains a complex issue and no predominant influence of the climate system can be determined. The stratosphere however seems to play a significant role for the NAO variability and more understanding of stratospheric dynamics and an improved monitoring of its behaviour could be helpful for the prediction of the NAO related fraction of variability (Maycock et al. (2009) also noted this).

The observed upward trend of the NAO index during our period of interest (1961-2002, see Section 4.2.1) is found to be best reproduced by the experiments with prescribed extratropical SSTSI (in OBS-NO and OBS-TROP20) which yield at least 30% of the magnitude of the observed NAO trend. Tropical relaxation adds some skill to the representation of the trend. When looking at the sub-period 1965-1995, stratospheric trends were found to have a considerable contribution to the observed upward trend in the NAO index (in agreement with Scaife et al., 2005), comparable with the contribution from SSTSI, while this signal is lost when looking at the whole period 1961 to 2002. This suggests that the atmospheric conditions in either of the two periods are not directly comparable on decadal time scales and conclusions taken from any 30 or 40-year-period can not be assumed to be universally valid.

In the North Pacific sector the tropical atmosphere and the tropical SST conditions during winter are the most important factors for the interannual variability (of the PNA) according to our experiments. It was found that especially constraining the tropical atmosphere to reanalysis data (CLIM-TROP and OBS-TROP20) powerfully enhances the model performance in general (Section 4.1, Figure 4.4) and also the PNA related part of the variability in this sector in particular (Section 4.1.2, Figures 4.9 and 4.10). This is consistent with the strong connection between the PNA and the tropical Pacific which was confirmed in a number of previous studies. The connection is caused by the poleward propagation of circulation anomalies through the upper troposphere causing an anomalous lower tropospheric circulation and also anomalous SST conditions in the extratropical North Pacific, called an "Atmospheric Bridge" (Alexander et al., 2002; Newman et al., 2003). It has to be noted that there is little representation of the observed PNA in the OBS-NO ensemble in the first third of our analysis period (see Figure 4.9), a fact that might be explained by a poor SSTSI observational data quality before the beginning of the satellite era.

The regime shift of the PNA (and related features) to a more positive state was found to possibly be caused by trends in the tropical atmosphere

(see Section 4.2.2, Figure 4.16, CLIM-TROP). This agrees with a trend to a higher occurrence of warm El Niño events, which are known to cause a deeper than usual Aleutian low (Alexander et al., 2002), in the second half of our period of interest. But also internal atmospheric variability clearly captures the overall trend between 1961 and 2002 (see Figure 4.16). Prescribing observed SST causes an opposite PNA trend compared to the observations, suggesting that this forcing degrades the model's ability to reproduce the PNA trend. This result could however be misleading because the atmospheric response to SST anomalies in atmosphere-only models (like ours) can in some regions be of the opposite sign relative to the observations (see Copsey et al., 2006). The tropical relaxation however (CLIM-TROP, OBS-TROP20) simulates a perfect coupling of ocean and atmosphere in the tropics and therefore is a good alternative to prescribing tropical SST in an AGCM.

There are a lot of possibilities for further experiments to be looked at, for example relaxing only parts of the tropics or only the tropical troposphere; also the impact of the extratropics on the tropics can be examined (see Jung et al., 2010, 2011; Vitart and Jung, 2010, for further possibilities). More analysis could be done, for example taking a closer look at running trends during sub-periods like that between 1965 and 1995, at the variability within the stratosphere or the evolution of specific winters like the cold European winter 1962/63 or the high NAO/low PNA winter of 1988/89.

List of Figures

List of Tables

Bibliography

Alexander, M. (1992). Midlatitude atmosphere-ocean interaction during El Niño. Part II: The northern hemisphere atmosphere. *Journal of Climate*, 5:959–972.

Alexander, M. A., Bladé, I., Newman, M., Lanzante, J. R., Lau, N.-C., and Scott, J. D. (2002). The Atmospheric Bridge: The influence of ENSO teleconnections on air-sea interaction over the global oceans. *Journal of Climate*, 15(16):2205–2231.

Baldwin, M. P. and Dunkerton, T. J. (2001). Stratospheric harbingers of anomalous weather regimes. *Science (New York, N.Y.)*, 294(5542):581–4.

Baldwin, M. P., Stephenson, D. B., and Jolliffe, I. T. (2009). Spatial weighting and iterative projection methods for EOFs. *Journal of Climate*, 22(2):234–243.

Barnston, A. and Livezey, R. (1987). Classification, seasonality and persistence of low-frequency atmospheric circulation patterns. *Monthly Weather Review*, 115(6):1083–1126.

Boer, G. J. and Hamilton, K. (2008). QBO influence on extratropical predictive skill. *Climate Dynamics*, 31(7-8):987–1000.

Bretherton, C. S. and Battisti, D. S. (2000). An interpretation of the results from atmospheric general circulation models forced by the time history of the observed sea surface temperature distribution. *Geophysical Research Letters*, 27(6):767.

Challinor, A. J., Wheeler, T. R., Slingo, J. M., Craufurd, P. Q., and Grimes, D. I. F. (2005). Simulation of crop yields using ERA-40: Limits to skill and nonstationarity in weather-yield relationships. *Journal of Applied Meteorology*, 44(4):516–531.

Copsey, D., Sutton, R., and Knight, J. R. (2006). Recent trends in sea level pressure in the Indian Ocean region. *Geophysical Research Letters*, 33(19):1–5.

Dommenget, D. and Latif, M. (2002). A cautionary note on the interpretation of EOFs. *Journal of Climate*, 15(2):216–225.

Fueglistaler, S., Dessler, A., Dunkerton, T., Folkins, I., Fu, Q., and Mote, P. (2009). Tropical tropopause layer. *Reviews of Geophysics*, 47(2008):1–31.

Greatbatch, R. J. (2000). The North Atlantic Oscillation. *Stochastic Environmental Research and Risk Assessment*, 14(4):0213–0242.

Greatbatch, R. J. and Jung, T. (2007). Local versus tropical diabatic heating and the winter North Atlantic Oscillation. *Journal of Climate*, 20(10):2058–2075.

Greatbatch, R. J., Lu, J., and Peterson, K. A. (2004). Nonstationary impact of ENSO on Euro-Atlantic winter climate. *Geophysical Research Letters*, 31(2):4–7.

Hilmer, M. and Jung, T. (2000). Evidence for a recent change in the link between the North Atlantic Oscillation and Arctic sea ice export. *Geophysical Research Letters*, 27(7):989.

Hsu, P. L. and Robbins, H. (1947). Complete convergence and the law of large numbers. *Proceedings of the National Academy of*, 33(2):25–31.

Hurrell, J. W. (1995). Decadal trends in the North Atlantic Oscillation: Regional temperatures and precipitation. *Science*, 269(5224):676.

Hurrell, J. W., Hoerling, M. P., Phillips, A. S., and Xu, T. (2004). Twentieth century North Atlantic climate change. Part I: Assessing determinism. *Climate Dynamics*, 23(3-4):371–389.

Hurrell, J. W., Kushnir, Y., Ottersen, G., and Visbeck, M. (2003). An overview of the North Atlantic oscillation. *Geophysical Monograph - American Geophysical Union*, 134:1–36.

Ineson, S. and Scaife, A. A. (2008). The role of the stratosphere in the European climate response to El Niño. *Nature Geoscience*, 2(1):32–36.

Jones, P. D., Jonsson, T., and Wheeler, D. (1997). Extension to the North Atlantic oscillation using early instrumental pressure observations from Gibraltar and south-west Iceland. *International Journal of Climatology*, 17(13):1433–1450.

Jung, T., Palmer, T. N., Rodwell, M. J., and Serrar, S. (2010). Understanding the anomalously cold European winter of 2005/06 using relaxation experiments. *Monthly Weather Review*, 138(8):3157–3174.

Jung, T., Vitart, F., Ferranti, L., and Morcrette, J.-J. (2011). Origin and predictability of the extreme negative NAO winter of 2009/10. *Geophysical Research Letters*, 38(7):1–6.

Klinker, E. (1990). Investigation of systematic errors by relaxation experiments. *Quarterly Journal of the Royal Meteorological Society*, 116(493):573–594.

Latif, M., Barnett, T., Cane, M., and Flügel, M. (1994). A review of ENSO prediction studies. *Climate Dynamics*, 9(4-5):167–179.

Lu, J., Greatbatch, R. J., and Peterson, K. A. (2004). Trend in northern hemisphere winter atmospheric circulation during the last half of the twentieth century. *Journal of Climate*, 17(19):3745–3760.

Mantua, N. J., Hare, S. R., Zhang, Y., Wallace, J. M., Francis, R. C., and Others (1997). A Pacific interdecadal climate oscillation with impacts on salmon production. *Bulletin of the American Meteorological Society*, 78(6):1069–1080.

Maycock, A. C., Keeley, S. P. E., Charlton-Perez, A. J., and Doblas-Reyes, F. J. (2009). Stratospheric circulation in seasonal forecasting models: Implications for seasonal prediction. *Climate Dynamics*, 36(1-2):309–321.

Metropolis, N. and Ulam, S. (1949). The Monte Carlo method. *Journal of the American Statistical Association*, 44(247):335–341.

Newman, M., Compo, G. P., and Alexander, M. A. (2003). ENSO-forced variability of the Pacific Decadal Oscillation. *Journal of Climate*, 16(23):3853–3857.

Peterson, K., Lu, J., and Greatbatch, R. (2003). Evidence of nonlinear dynamics in the eastward shift of the NAO. *Geophys. Res. Lett*, 30(2):1030.

Rayner, N. (2001). HadISST1 and the Reynolds et al. analysis. *ERA-40 Project Report Series*, 3:169–176.

Scaife, A. A., Knight, J. R., Vallis, G. K., and Folland, C. K. (2005). A stratospheric influence on the winter NAO and North Atlantic surface climate. *Geophysical Research Letters*, 32(18):1–5.

Semenov, V. A., Latif, M., Jungclaus, J. H., and Park, W. (2008). Is the observed NAO variability during the instrumental record unusual? *Geophysical Research Letters*, 35(11):1–5.

Stoner, A. M. K., Hayhoe, K., and Wuebbles, D. J. (2009). Assessing general circulation model simulations of atmospheric teleconnection patterns. *Journal of Climate*, 22(16):4348–4372.

Thompson, D. W. J. and Solomon, S. (2002). Interpretation of recent southern hemisphere climate change. *Science*, 296(5569):895–9.

Thompson, D. W. J. and Wallace, J. M. (1998). The Arctic Oscillation signature in the wintertime geopotential height and temperature fields. *Geophysical Research Letters*, 25(9):1297–1300.

Thompson, D. W. J., Wallace, J. M., and Hegerl, G. C. (2000). Annular Modes in the Extratropical Circulation. Part II: Trends. *Journal of Climate*, 13(5):1018–1036.

Trenberth, K. (1997). The definition of El Niño. *Bulletin of the American Meteorological Society*, 78(12):2771–2778.

Trenberth, K., Caron, J., Stepaniak, D., and Worley, S. (2002). Evolution of El Niño-Southern Oscillation and global atmospheric surface temperatures. *Journal of geophysical research*, 107(D8):4065.

Trenberth, K. and Hurrell, J. (1994). Decadal atmosphere-ocean variations in the Pacific. *Climate Dynamics*, 9(6):303–319.

Trenberth, K. E., Branstator, G. W., Karoly, D., Kumar, A., Lau, N.-C., and Ropelewski, C. (1998). Progress during TOGA in understanding and modeling global teleconnections associated with tropical sea surface temperatures. *Journal of Geophysical Research*, 103(C7):14291–14324.

Trenberth, K. E. and Caron, J. M. (2000). The Southern Oscillation revisited: Sea level pressures, surface temperatures, and precipitation. *Journal of Climate*, 13(24):4358–4365.

Uppala, S. M., Kallberg, P. W., Simmons, A. J., Andrae, U., Bechtold, V. D. C., Fiorino, M., Gibson, J. K., Haseler, J., Hernandez, A., Kelly, G. A., Li, X., Onogi, K., Saarinen, S., Sokka, N., Allan, R. P., Andersson, E., Arpe, K., Balmaseda, M. A., Beljaars, A. C. M., Berg, L. V. D., Bidlot, J., Bormann, N., Caires, S., Chevallier, F., Dethof, A., Dragosavac, M., Fisher, M., Fuentes, M., Hagemann, S., Hólm, E., Hoskins, B. J., Isaksen, L., Janssen, P. A. E. M., Jenne, R., Mcnally, A. P., Mahfouf, J.-F., Morcrette, J.-J., Rayner, N. A., Saunders, R. W., Simon, P., Sterl, A., Trenberth, K. E., Untch, A., Vasiljevic, D., Viterbo, P., and Woollen, J. (2005). The ERA-40 re-analysis. *Quarterly Journal of the Royal Meteorological Society*, 131(612):2961–3012.

Vitart, F. and Jung, T. (2010). Impact of the northern hemisphere extratropics on the skill in predicting the Madden Julian Oscillation. *Geophysical Research Letters*, 37(23):1–6.

von Storch, H. and Zwiers, F. W. (2001). *Statistical analysis in climate research*. Cambridge University Press, Cambridge.

Wallace, J. M. and Gutzler, D. S. (1981). Teleconnections in the 500 mb geopotential height field during the northern hemisphere winter. *Monthly Weather Review*, 109:784–812.

Wallace, J. M., Zhang, Y., and Renwick, J. A. (1995). Dynamic contribution to hemispheric mean temperature trends. *Science*, 270(5237):780–783.

Wunsch, C. (1999). The interpretation of short climate records, with comments on the North Atlantic and Southern Oscillations. *Bulletin of the American Meteorological Society*, 80(2):245–255.

Acknowledgements

I want to thank Prof. Dr. Richard Greatbatch for the outstanding supervision and support of this thesis.

I am also grateful to Prof. Dr. Thomas Jung from AWI Bremerhaven for the setup and the execution of the model experiments.

Torben Kunz gave helpful input on large parts of the analysis of the model output.

Many thanks to my good friend Martin Claus who was always available for interesting discussions of the results, who helped with a lot of technical know-how and was a constant companion through all the years of studies.

Special thanks also to my parents who supported me during my studies at all times and in all aspects.

Last but not least, the Theorie and Modellierung department at IFM-GEOMAR was the perfect basis to write this thesis and offered many friendly colleagues and a pleasant working atmosphere.

Erklärung

Hiermit erkläre ich, dass ich die vorliegende Diplomarbeit selbständig verfasst und keine anderen als die angegebenen Quellen und Hilfsmittel verwendet habe. Ich versichere, dass diese Arbeit noch nicht an anderer Stelle zur Erlangung eines akademischen Grades vorgelegen hat.

Kiel, Dezember 2011,

(Gereon Gollan)